JPET Fast Forward. Published on May 4, 2017 as DOI: 10.1124/jpet.116.239590
This article has not been copyedited and formatted. The final version may differ from this version.

Pharmacologic Characterization of AMG8379, a Potent and Selective Small Molecule Sulfonamide Antagonist of the Voltage-Gated Sodium Channel $Na_V1.7$

Thomas J. Kornecook, Ruoyuan Yin, Stephen Altmann, Xuhai Be, Virginia Berry, Christopher P. Ilch, Michael Jarosh, Danielle Johnson, Josie H. Lee, Sonya G. Lehto, Joseph Ligutti, Dong Liu, Jason Luther, David Matson, Danny Ortuno, John Roberts, Kristin Taborn, Jinti Wang, Matthew M. Weiss, Violeta Yu, Dawn X. D. Zhu, Robert T. Fremeau Jr., and Bryan D. Moyer*

Department of Neuroscience (S.A, R.T.F, C.P.I., M.J., D.J., T.K., J.H.L., S.L., J.L., J.L, D.L., D.M., B.D.M., D.O., K.T., J.W., R.Y., V.Y., D.Z.), Department of Medicinal Chemistry (M. W.), and Department of Pharmacokinetics and Drug Metabolism (X.B., V.B., J.R.), Amgen Inc., 360 Binney Street, Cambridge, Massachusetts 02142, and One Amgen Center Drive, Thousand Oaks, CA 91320, United States.

Running title: Pharmacology of the novel $Na_V1.7$ antagonist AMG8379

*Corresponding author:

Bryan D. Moyer

Amgen, Inc.

One Amgen Center Drive

MS 29-2-B

Thousand Oaks, CA 91320

Phone: 1-805-313-5495

FAX: 1-805-499-9835

E-Mail: bmoyer@amgen.com

Number of text pages: 60

Number of tables: 3

Number of figures: 10

Number of references: 67

Number of words in Abstract: 246

Number of words in Introduction: 642

Number of words in Discussion: 1552

Abbreviations: CHO, Chinese hamster ovary; DMEM, Dulbecco's modified Eagle's medium; DRG, dorsal root ganglia; FBS, fetal bovine serum; HEK, human embryonic kidney; IWQ, IonWorks Quattro, MEM, minimal essential medium; NEAA, non-essential

amino acids; PX, PatchXpress, TTX, tetrodotoxin; TTX-R, tetrodotoxin-resistant; TTX-S, tetrodotoxin-sensitive

Recommended section assignment: Neuropharmacology

JPET Fast Forward. Published on May 4, 2017 as DOI: 10.1124/jpet.116.239590
This article has not been copyedited and formatted. The final version may differ from this version.

Abstract

Potent and selective antagonists of the voltage-gated sodium channel $Na_V1.7$ represent a promising avenue for the development of new chronic pain therapies. We generated a small molecule atropisomer quinolone sulfonamide antagonist AMG8379 and a less active enantiomer AMG8380. Here we show that AMG8379 potently blocks human $Na_V1.7$ channels with an IC_{50} of 8.5 nM and endogenous tetrodotoxin (TTX)-sensitive sodium channels in dorsal root ganglia (DRG) neurons with an IC_{50} of 3.1 nM in whole cell patch clamp electrophysiology assays using a voltage protocol that interrogates channels in a partially inactivated state. AMG8379 was 100 to 1000-fold selective over other Na_V family members, including $Na_V1.4$ expressed in muscle and $Na_V1.5$ expressed in heart, as well as TTX-resistant Na_V channels in DRG neurons. Using an *ex vivo* mouse skin-nerve preparation, AMG8379 blocked mechanically-induced action potential firing in C-fibers in both a time-dependent and dose-dependent manner. AMG8379 similarly reduced the frequency of thermally-induced C-fiber spiking, whereas AMG8380 affected neither mechanical nor thermal responses. In vivo target engagement of AMG8379 in mice was evaluated in multiple $Na_V1.7$-dependent behavioral endpoints. AMG8379 dose-dependently inhibited intradermal histamine-induced scratching and intraplantar capsaicin-induced licking, and reversed UVB radiation skin burn-induced thermal hyperalgesia; notably, behavioral effects were not observed with AMG8380 at similar plasma exposure levels. AMG8379 is a potent and selective $Na_V1.7$ inhibitor that blocks sodium current in heterologous cells as well as DRG neurons, inhibits action potential firing in peripheral nerve fibers, and exhibits pharmacodynamic effects in translatable models of both itch and pain.

JPET Fast Forward. Published on May 4, 2017 as DOI: 10.1124/jpet.116.239590
This article has not been copyedited and formatted. The final version may differ from this version.

Introduction

Chronic pain represents a critical unmet medical need that afflicts over one hundred million Americans with an economic cost over $500 billion (Pizzo, 2011; Holmes, 2016). Despite the fact that the chronic pain market landscape in the United States, Europe, and Japan represents over $21 billion, current available therapies lack robust efficacy, carry significant abuse potential, and/or suffer from low tolerability and safety; numbers needed to treat, corresponding to the number of individuals receiving a treatment for one individual to achieve 50% or greater pain relief, range between four and ten for current therapies (Taylor, 2013; Finnerup et al., 2015). Between 2009 and 2014, thirty-three potential drugs for neuropathic pain, a form of chronic pain arising from damage to the somatosensory system that is particularly recalcitrant to treatment, were discontinued in clinical trials, highlighting the urgent need to identify both new targets as well as develop new therapeutics for pain indications (Knezevic et al., 2015).

$Na_V1.7$ is a TTX-sensitive voltage-gated sodium ion channel that regulates action potential firing in nociceptor neurons within the peripheral nervous system (Klugbauer et al., 1995; Cummins et al., 1998; Black et al., 2012; Dib-Hajj et al., 2013). Sodium influx through $Na_V1.7$ generates ramp currents that can boost sub-threshold depolarizing stimuli toward the threshold required to trigger sensory neuron action potentials, and $Na_V1.7$ also contributes to the upstroke of nociceptor action potentials (Cummins et al., 1998; Rush et al., 2007; Alexandrou et al., 2016). In addition to its peripheral expression profile and role in action potential initiation, $Na_V1.7$ represents a particularly compelling target for the development of chronic pain therapies due to its robust human genetic validation. Loss-of-function mutations lead to congenital insensitivity to pain

JPET Fast Forward. Published on May 4, 2017 as DOI: 10.1124/jpet.116.239590
This article has not been copyedited and formatted. The final version may differ from this version.

(Cox et al., 2006; Goldberg et al., 2007), whereas gain-of-function mutations lead to pain in primary erythromelalgia, paroxysmal extreme pain disorder, and small fiber neuropathy (Yang et al., 2004; Fertleman et al., 2006; Faber et al., 2012). Furthermore, in mice, genetic knockout of $Na_V1.7$ in specific neuronal populations mitigates pain behavior following both inflammatory and nerve injury insults (Nassar et al., 2004; Minett et al., 2012), while global knockout of $Na_V1.7$ from birth recapitulates the human phenotype of congenital insensitivity to pain (Gingras et al., 2014).

$Na_V1.7$ has been the intense focus of research activities to identify inhibitors for therapeutic development for chronic pain (Bagal et al., 2014; Sun et al., 2014a; de Lera Ruiz and Kraus, 2015; Emery et al., 2016; Vetter et al., 2016). Amongst these endeavors, sulfonamide-based small molecule antagonists have emerged as potent and selective compounds that block $Na_V1.7$, with greatly reduced potency against homologous sodium channels including $Na_V1.5$ expressed in the heart. Mechanistically, block is achieved by engaging a novel binding pocket located within the fourth voltage-sensor domain and stabilizing $Na_V1.7$ in an inactivated conformation, thereby preventing channels from efficiently recycling to the resting/closed state and reducing availability for subsequent opening events (McCormack et al., 2013; Sun et al., 2014b; Ahuja et al., 2015; Alexandrou et al., 2016; Focken et al., 2016; Theile et al., 2016). Poor inhibition of rat $Na_V1.7$ channels by this chemotype is attributed to amino acid sequence differences in this region (McCormack et al., 2013; Alexandrou et al., 2016; Focken et al., 2016). Specific interaction with the fourth voltage-sensor domain differentiates the sulfonamide binding site from previously described Na_V binding sites for toxin-derived peptides, local anesthetics, and tetrodotoxin (de Lera Ruiz and Kraus, 2015).

Here, we describe an extensive *in vitro*, *ex vivo*, and *in vivo* pre-clinical pharmacological characterization of the novel sulfonamide $Na_V1.7$ antagonist AMG8379 and its significantly less active enantiomer AMG8380 which serves as a negative control. AMG8379 represents a potent and selective $Na_V1.7$ inhibitor that blocks action potential firing in peripheral nerve fibers and displays efficacy in translatable mouse models of both itch and pain, whereas the less active enantiomer AMG8380 is devoid of these biological effects at comparable plasma concentrations.

Materials and Methods

Cell Lines. Human $Na_V1.1$ human embryonic kidney 293 (HEK293), $Na_V1.2$ and $Na_V1.3$ Chinese hamster ovary (CHO), $Na_V1.4$ HEK293, $Na_V1.5$ HEK293, $Na_V1.6$ HEK293, and $Na_V1.7$ HEK293 stable cell lines were purchased from Eurofins Pharma Discovery Services. $Na_V1.1$, $Na_V1.4$, $Na_V1.5$ and $Na_V1.7$ cell lines were maintained in Dulbecco's modified Eagle's medium (DMEM)/F12 supplemented with certified fetal bovine serum (FBS) 10% v/v, 1% minimal essential medium (MEM) nonessential amino acids, 100 units/ml Penicillin, 100 μg/ml streptomycin and 0.292 mg/ml of L-glutamine (Gibco Life Technologies). $Na_V1.2$ and $Na_V1.3$ cell lines were maintained in Iscove's Modified Dulbecco's medium supplemented with dialyzed FBS 10% v/v, 1 % HT supplement, 1% MEM nonessential amino acids, 100 units/ml Penicillin, 100 μg/ml streptomycin and 0.292 mg/ml of L-glutamine (Gibco Life Technologies). All cell lines were maintained at 37°C in a humidified 95% O_2/5% CO_2 atmosphere in the presence of the selection antibiotic geneticin 400 μg/ml (Gibco Life Technologies). U-2 OS cells were maintained and transduced at 200 MOI with mouse $Na_V1.1$ or mouse $Na_V1.6$ BacMam viruses as previously described (Liu et al., 2016). For routine passaging cells were lifted with 0.05% Trypsin-EDTA (Gibco Life Technologies) and grown in T-75 or T-150 Flasks (Corning) to 50-80% confluency to prevent contact inhibition of channel expression. Mouse and rat $Na_V1.7$ sequences were sub-cloned into the antibiotic selection vector pSLX240h, linearized and stably transfected using Lipofectamine LTX into HEK293 (for mouse $Na_V1.7$) or HEK293T (for rat $Na_V1.7$). Following 48-72 h of transfection, media containing 80 ug/mL hygromycin was added and selection was

JPET Fast Forward. Published on May 4, 2017 as DOI: 10.1124/jpet.116.239590
This article has not been copyedited and formatted. The final version may differ from this version.

continued for 24-30 d. Individual colonies were picked into 96 well plates, expanded, and expression was confirmed by electrophysiology testing.

Experimental Procedures for the Preparation of AMG8379 and AMG8380.

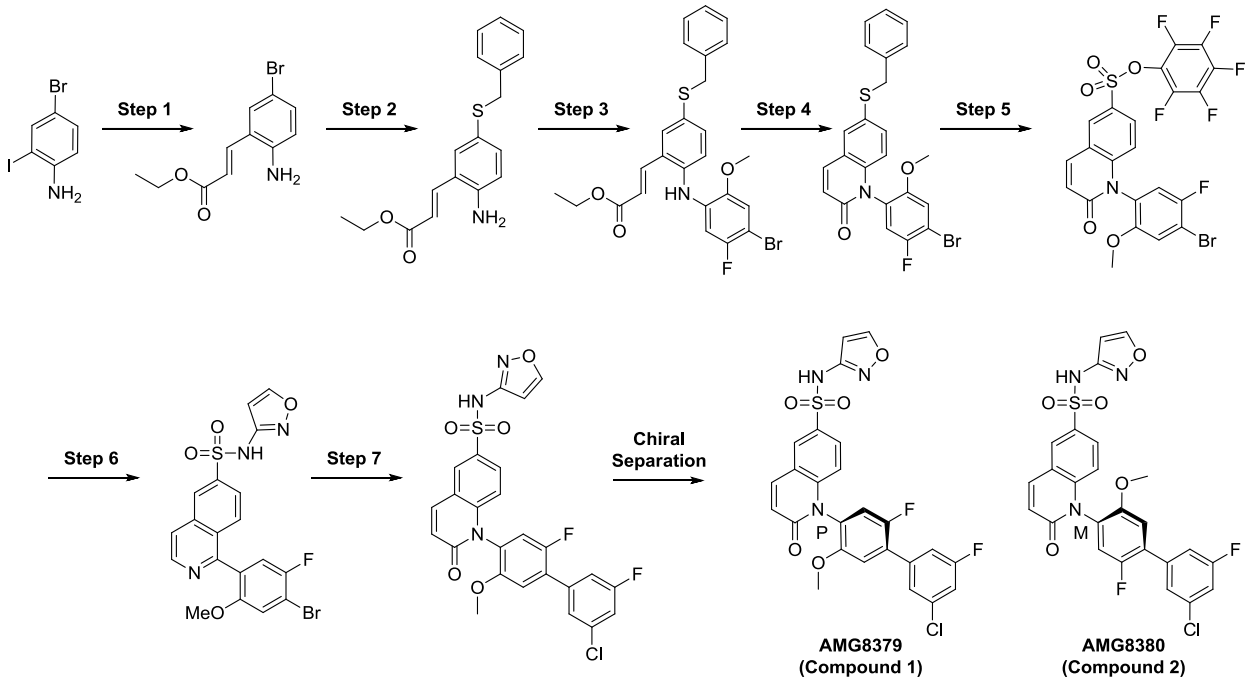

Step 1:

(E)-ethyl 3-(2-amino-5-bromophenyl)acrylate

To a solution of 4-bromo-2-iodoaniline (25.0 g, 84 mmol) in DMF (56.0 mL) was added ethyl acrylate (8.8 g, 88 mmol) and sodium bicarbonate (17.62 g, 210 mmol). The reaction mixture was degassed with nitrogen for 20 minutes followed by the addition of palladium acetate (0.94 g, 4.20 mmol). The reaction mixture was heated at 100 °C for 4 hours. The reaction was filtered through celite and the celite bed was

JPET Fast Forward. Published on May 4, 2017 as DOI: 10.1124/jpet.116.239590
This article has not been copyedited and formatted. The final version may differ from this version.

washed with ethyl acetate (2 x 500 mL). The filtrate was concentrated under reduced pressure to obtain a crude residue which was purified by column chromatography (silica gel; mesh size 60-120, elution 0-20% ethyl acetate in hexanes) to obtain (E)-ethyl 3-(2-amino-5-bromophenyl)acrylate (20.4 g, 90 %), as yellow solid. MS (ESI, positive ion) m/z; 271.2 (M+1). ^{1}H NMR (400 MHz, DMSO) δ 7.75 (d, *J* = 16.1 Hz, 1H), 7.57 (d, *J* = 2.0 Hz, 1H), 7.16 (dd, *J* = 9.1, 2.4 Hz, 1H), 6.66 (d, *J* = 8.6 Hz, 1H), 6.43 (d, *J* = 8.6 Hz, 1H), 5.81 (s, 2H), 4.20 (q, *J* = 7.2 Hz, 2H), 1.27 (t, *J* = 7.2 Hz, 3H).

Step 2:

(E)-ethyl 3-(2-amino-5-(benzylthio)phenyl)acrylate

To a solution of (E)-ethyl 3-(2-amino-5-bromophenyl)acrylate (20.0 g, 74 mmol) in 1,4-dioxane (74 mL) was added DIPEA (25.8 mL, 148 mmol). The solution was degassed with nitrogen for 20 mins at which point XantPhos (2.14 g, 3.70 mmol), and $Pd_2(dba)_3$ (1.67 g, 1.85 mmol) was added to the reaction mixture. The mixture was purged with nitrogen and heated to 80 °C for 30 minutes. The reaction was cooled to room temperature and benzyl mercaptan (9.66 g, 78 mmol) was added and the reaction was heated at 80 °C for an additional 2 hours. The reaction was cooled to room temperature and diluted with ethyl acetate. The mixture was filtered through celite and the celite bed was washed with ethyl acetate. The filtrate was concentrated under reduced pressure to obtain the crude material which was purified by chromatography (silica gel; mesh size 60-120, elution 0-40% ethyl acetate and heptane) to obtain (E)-ethyl 3-(2-amino-5-(benzylthio)phenyl)acrylate (21.4 g, 92%), as yellow solid. MS (ESI,

positive ion) m/z; 314.1 (M+1). ^{1}H NMR (400 MHz, DMSO) δ 7.79 (d, *J* = 16.1 Hz, 1H), 7.37 (d, *J* = 2.0 Hz, 1H), 7.25 – 7.17 (m, 5H) 7.10 (dd, *J* = 8.4, 2.1 Hz, 1H), 6.61 (d, *J* = 8.3 Hz, 1H), 6.32 (d, *J* = 15.2 Hz, 1H), 5.75 (s, 2H), 4.20 (q, *J* = 7.2 Hz, 2H), 4.01 (s, 2H), 1.27 (t, *J* = 7.2 Hz, 3H).

Step 3:

(E)-ethyl 3-(5-(benzylthio)-2-((4-bromo-5-fluoro-2-methoxyphenyl)amino)phenyl)acrylate

To a solution of (E)-ethyl 3-(2-amino-5-(benzylthio)phenyl)acrylate (5.00 g, 15.9 mmol) and 1-bromo-2-fluoro-4-iodo-5-methoxybenzene (6.34 g, 19.1 mmol) in CPME (32 m L) was added Cs_2CO_3 (7.28 g, 22.3 mmol) and the mixture was degassed with nitrogen for 20 mins. $Pd_2(dba)_3$ (0.37 g, 0.40 mmol) and XantPhos (0.46 g, 0.80 mmol) were added to the reaction mixture and the mixture was heated at 90 °C for 3 hours. The reaction mixture was allowed to cool to room temperature, diluted with ethyl acetate and filtered through celite. The filtrate was concentrated under reduced pressure to obtain the crude material which was purified by stirring with isopropanol for 16 hours and filtered to obtain (E)-ethyl 3-(5-(benzylthio)-2-((4-bromo-5-fluoro-2-methoxyphenyl)amino)phenyl)acrylate (7.27 g, 88 %) as yellow solid. MS (ESI, positive ion) m/z; 516.2 (M+1). ^{1}H NMR (400 MHz, DMSO) δ 7.73 – 7.61 (m, 3H), 7.34 – 7.15 (m, 6H), 7.02 (d, *J* = 11.4 Hz, 1H), 6.60 (d, *J* = 21.2 Hz, 1H), 6.33 (d, *J* = 14.1 Hz, 1H), 4.26 (s, 2H), 4.16 – 4.09 (m, 2H), 3.81 (s, 3H), 1.22 (t, *J* = 7.2 Hz, 3H).

JPET Fast Forward. Published on May 4, 2017 as DOI: 10.1124/jpet.116.239590
This article has not been copyedited and formatted. The final version may differ from this version.

Step 4:

6-(benzylthio)-1-(4-bromo-5-fluoro-2-methoxyphenyl)quinolin-2(1H)-one

A round-bottom flask was charged with (E)-ethyl 3-(5-(benzylthio)-2-((4-bromo-5-fluoro-2-methoxyphenyl)amino)phenyl)acrylate (7.27 g, 14.08 mmol) and MeOH (70.4 ml) to give a yellow suspension. Sodium methoxide (25 wt% in MeOH) (1.25 ml, 5.63 mmol) was added. A reflux condenser was attached, and the flask was lowered into a 70 °C heating bath. After 4 hours, the mixture was cooled and concentrated under vacuum to obtain the crude material which was purified by stirring with isopropanol for 16 hours and filtered to give 6-(benzylthio)-1-(4-bromo-5-fluoro-2-methoxyphenyl)quinolin-2(1H)-one (6.05 g, 91 % yield). MS (ESI, positive ion) m/z; 470.0 (M+1). ^{1}H NMR (400 MHz, DMSO) δ 7.92 (d, *J* = 9.1 Hz, 1H), 7.79 (d, *J* = 1.7 Hz, 1H), 7.65 (d, *J* = 6.1 Hz, 1H), 7.57 (d, *J* = 8.8 Hz, 1H), 7.40 – 7.22 (m, 6H), 6.68 (d, *J* = 9.6 Hz, 1H), 6.56 (d, *J* = 8.8 Hz, 1H), 4.24 (s, 2H), 3.69 (s, 3H).

Step 5:

Perfluorophenyl 1-(4-bromo-5-fluoro-2-methoxyphenyl)-2-oxo-1,2-dihydroquinoline-6-sulfonate

To a solution of 6-(benzylthio)-1-(4-bromo-5-fluoro-2-methoxyphenyl)quinolin-2(1H)-one (6.00 g, 12.76 mmol) in acetonitrile (40.0 mL) were added acetic acid (1.5 mL) and water (1.0 mL). The resulting mixture was cooled to 0 ^{o}C and 1,3-dichloro-5,5-dimethylimidazolidine-2,4-dione (2.64 g, 13.4 mmol) was added portion-wise over 20

JPET Fast Forward. Published on May 4, 2017 as DOI: 10.1124/jpet.116.239590
This article has not been copyedited and formatted. The final version may differ from this version.

minutes keeping the internal temperature below 5ºC. The resulting suspension was stirred at 0-5°C under nitrogen for 45 min. Then pentafluorophenol (2.82 g, 15.31 mmol) was added followed by NEt_3 (7.11 mL, 51.0 mol). The mixture was continued to be stirred at 0-5 ºC for 30 minutes. Water was added and extracted with ethyl acetate. The organic layer was washed with brine, dried over sodium sulfate, filtered and concentrated under reduced pressure to obtain the crude product which was purified by stirring with isopropyl alcohol : hexanes (1:1) and filtered to obtain perfluorophenyl 1-(4-bromo-5-fluoro-2-methoxyphenyl)-2-oxo-1,2-dihydroquinoline-6-sulfonate (6.05 g, 80%) as white solid. MS (ESI, positive ion) m/z; 594.2 (M+1). ^{1}H-NMR (400 MHz, DMSO) δ 8.60 (d, *J* = 2.0 Hz, 1H), 8.26 (d, *J* = 9.8 Hz, 1H), 7.95 (dd, *J* = 2.2, 9.1 Hz, 1H), 7.70 (t, *J* = 8.6 Hz, 2H), 6.95 - 6.88 (m, 2H), 3.72 (s, 3H).

Step 6:

1-(4-bromo-5-fluoro-2-methoxyphenyl)-N-(isoxazol-3-yl)-2-oxo-1,2-dihydroquinoline-6-sulfonamide

A THF (50 mL) solution of perfluorophenyl 1-(4-bromo-5-fluoro-2-methoxyphenyl)-2-oxo-1,2-dihydroquinoline-6-sulfonate (3.00 g, 5.05 mmol) and 3-aminoisoxazole (0.41 ml, 5.55 mmol) in a 250-mL round-bottom flask was cooled to 0 °C, and lithium bis(trimethylsilyl)amide, 1.0 M solution in THF (10.6 ml, 10.6 mmol) was added dropwise. After stirring the solution at 0 °C for 1 hour, the reaction was quenched at 0 °C with 1 N HCl and extracted thrice with EtOAc. The organic extracts were combined, dried over MgSO4, filtered, and concentrated to a light tan residue,

JPET Fast Forward. Published on May 4, 2017 as DOI: 10.1124/jpet.116.239590
This article has not been copyedited and formatted. The final version may differ from this version.

affording 3.81 g of the product. The resulting filtrate was concentrated under reduced pressure to obtain the crude product which was purified by stirring with ethyl acetate and filtered to obtain 1-(4-bromo-5-fluoro-2-methoxyphenyl)-N-(isoxazol-3-yl)-2-oxo-1,2-dihydroquinoline-6-sulfonamide 2.08 g, 83 % yield) was afforded as an off-white solid. m/z (ESI) 494.1 $(M+H)^+$. ^{1}H NMR (400MHz, DMSO-d_6) δ = 11.66 (br. s., 1 H), 8.72 (d, *J* = 1.8 Hz, 1 H), 8.35 (d, *J* = 2.2 Hz, 1 H), 8.21 (d, *J* = 9.6 Hz, 1 H), 7.83 (dd, *J* = 2.2, 8.9 Hz, 1 H), 7.52 (s, 1 H), 7.34 (d, *J* = 0.4 Hz, 1 H), 6.78 (d, *J* = 9.6 Hz, 2 H), 6.43 (d, *J* = 1.9 Hz, 1 H), 3.67 (s, 3 H).

Step 7:

(P)-1-(3'-chloro-2,5'-difluoro-5-methoxy-4-biphenylyl)-N-3-isoxazolyl-2-oxo-1,2-dihydro-6-quinolinesulfonamide (Compound 1; AMG8379) and **(M)-1-(3'-chloro-2,5'-difluoro-5-methoxy-4-biphenylyl)-N-3-isoxazolyl-2-oxo-1,2-dihydro-6-quinolinesulfonamide (Compound 2: AMG8380)**

A screw cap vial was charged with 1-(4-bromo-5-fluoro-2-methoxyphenyl)-N-(isoxazol-3-yl)-2-oxo-1,2-dihydroquinoline-6-sulfonamide (2.00 g, 4.05 mmol), (3-chloro-5-fluorophenyl)boronic acid (1.058 g, 6.07 mmol), potassium carbonate (1.678 g, 12.14 mmol) and $Pd(Ph_3P)_4$ (0.468 g, 0.405 mmol). The vial was flushed with Ar (g) and then 1,4-dioxane (15 mL) and water (5 mL) were added in sequence. The reaction was heated to 90 °C for 3 hours. The mixture was diluted with NH_4Cl and extracted with EtOAc (3x).The combined organic extracts were dried over magnesium sulfate, filtered, and concentrated. The residue was purified by chromatography on silica gel (40-g Ultra

JPET Fast Forward. Published on May 4, 2017 as DOI: 10.1124/jpet.116.239590
This article has not been copyedited and formatted. The final version may differ from this version.

SNAP column, 25-g silica gel loading column, 0-50% EtOAc/Heptane) to give 1-(3'-chloro-2,5'-difluoro-5-methoxy-4-biphenylyl)-N-3-isoxazolyl-2-oxo-1,2-dihydro-6-quinolinesulfonamide (1.85 g, 84 % yield) as a cream-colored solid. m/z (ESI) 544.2 $(M+H)^+$.

Chiral Separation:

Racemic 1-(3'-chloro-2,5'-difluoro-5-methoxy-4-biphenylyl)-N-3-isoxazolyl-2-oxo-1,2-dihydro-6-quinolinesulfonamide was subjected to chiral separation by SFC using an AS-H column (25% MeOH/75% CO_2) to give (P)-1-(3'-chloro-2,5'-difluoro-5-methoxy-4-biphenylyl)-N-3-isoxazolyl-2-oxo-1,2-dihydro-6-quinolinesulfonamide (Compound 1; AMG8379) as peak 1 and (M)-1-(3'-chloro-2,5'-difluoro-5-methoxy-4-biphenylyl)-N-3-isoxazolyl-2-oxo-1,2-dihydro-6-quinolinesulfonamide as peak 2 (Compound 2; AMG8380). Data for peak 1: ^{1}H NMR (500 MHz, DMSO-d_6) δ 11.56-11.84 (br s, 1H), 11.56-11.84 (m, 1H), 8.71 (d, *J*=1.60 Hz, 1H), 8.37 (d, *J*=1.87 Hz, 1H), 8.23 (d, *J*=9.67 Hz, 1H), 7.86 (dd, *J*=2.00, 8.95 Hz, 1H), 7.66 (s, 1H), 7.53-7.63 (m, 3H), 7.47 (d, *J*=6.84 Hz, 1H), 6.86 (d, *J*=8.98 Hz, 1H), 6.81 (d, *J*=9.67 Hz, 1H), 3.75 (s, 3H). m/z (ESI) 542.1 $(M-H)^-$. Data for Peak 2: ^{1}H NMR (500 MHz, DMSO-d_6) δ 11.39-11.86 (br s, 1H), 8.71 (d, *J*=1.55 Hz, 1H), 8.37 (d, *J*=1.87 Hz, 1H), 8.23 (d, *J*=9.72 Hz, 1H), 7.85 (dd, *J*=2.06, 8.90 Hz, 1H), 7.66 (s, 1H), 7.51-7.63 (m, 3H), 7.47 (d, *J*=6.89 Hz, 1H), 6.85 (d, *J*=9.03 Hz, 1H), 6.81 (d, *J*=9.67 Hz, 1H), 6.44 (d, *J*=1.55 Hz, 1H), 3.75 (s, 4H). m/z (ESI) 542.1 $(M-H)^-$.

JPET Fast Forward. Published on May 4, 2017 as DOI: 10.1124/jpet.116.239590
This article has not been copyedited and formatted. The final version may differ from this version.

The $Na_V1.8$ blocker compound 31 was from (Kort et al., 2010).

Radioligand Binding Assay. Binding of AMG8379 and AMG8380 to membranes from human $Na_V1.7$ HEK293 cells was performed as previously described (DiMauro et al., 2016) using the tritiated sulfonamide radioligand **4** described below.

Preparation of Radiolabeled Sulfonamide ((P)-1-(3-chloro-2-fluoro-5,5-dimethoxy-[1,1-biphenyl]-4-yl)-N-(isoxazol-3-yl)-2-oxo-1,2-dihydroquinoline-6-sulfonamide [5-methoxy-C^3H_3].

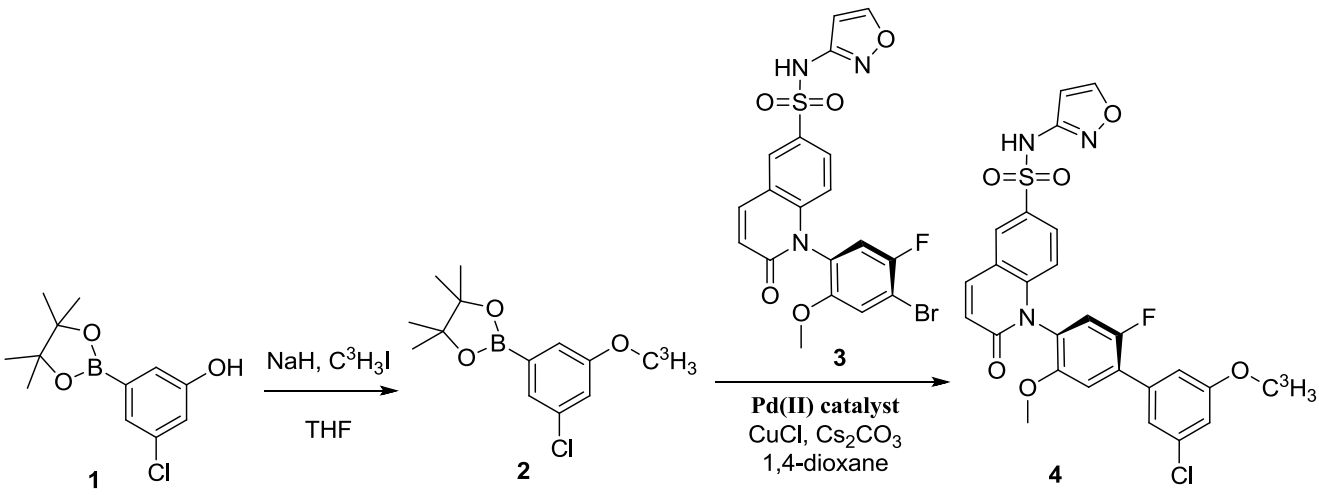

JPET Fast Forward. Published on May 4, 2017 as DOI: 10.1124/jpet.116.239590
This article has not been copyedited and formatted. The final version may differ from this version.

NaH (60% dispersion in mineral oil, 15.8 mg, 395 μmol) was weighed into a flask and washed twice with *n*-heptane (1 mL). Dry THF (1.00 mL) was added, followed by a solution of compound 1 (3-chloro-5-(4,4,5,5-tetramethyl-1,3,2-dioxaborolan-2-yl)phenol) (33.5 mg, 132 μmol) in dry THF (0.50 mL). The mixture was allowed to stir for 20 min at room temperature under a nitrogen atmosphere at which time a solution of C^3H_3I (400 mCi, 6.5 μmol) in dry THF (0.5 mL) was added. The reaction mixture was stirred at room temperature for 36 hours before being diluted with dichloromethane (1.0 mL) and filtered through celite. The clear organic solution was concentrated to provide compound 2 (2-(3-chloro-5-methoxyphenyl)-4,4,5,5-tetramethyl-1,3,2-dioxaborolane [5-methoxy-C^3H_3]) which was subsequently dissolved in 1,4-dioxane (0.2 mL). To this solution was added Cs_2CO_3 (11.8 mmol, 36.2 μmol), CuCl (2.68 mg, 27.1 μmol), compound 3* ((P)-1-(4-bromo-5-fluoro-2-methoxyphenyl)-N-(isoxazol-3-yl)-2-oxo-1,2-dihydroquinoline-6-sulfonamide) (4.91 mg, 9.93 μmol) and bis(di-tert-butyl(4-dimethylaminophenyl)phosphine)dichloropalladium(II) (1.92 mg, 2.71 μmol). The mixture was stirred at 50 ^oC for 5 hours. The reaction was cooled to room temperature, filtered through celite and washed with MeOH (10 mL). The filtrate was concentrated under reduced pressure, and the residue was purified by preparative HPLC [Waters X-Bridge C18; 10.0 × 150 mm, 5 μm; Mobile phase A: 0.1% TFA water, Mobile phase B: 0.1% TFA acetonitrile; Gradient: (min, B%) = (0, 40) → (20, 100) → (25, 100) → (25.1, 40) → (30, 40) ; 5.0 mL/min; 254 nm] to afford a solution of compound 4. To the derived solution of was added saturated aqueous $NaHCO_3$ (0.1 mL) and the mixture was loaded onto a BAKERBOND SPE™ C18 cartridge (J.T.Baker, catalog number 7020-06, 6 mL, 500 mg). The cartridge was rinsed with water and then the desired

JPET Fast Forward. Published on May 4, 2017 as DOI: 10.1124/jpet.116.239590
This article has not been copyedited and formatted. The final version may differ from this version.

product was eluted with ethanol to provide crude compound 4. This material was subsequently repurified *via* chiral preparative HPLC [CHIRALCELL OD-H; 4.6 × 250 mm, 5 µm; Mobile phase: TFA / *n*-heptane / EtOH = 0.2/75/25; 1.0 mL/min; 254 nm]. The combined fractions containing compound 4 were treated with saturated aqueous $NaHCO_3$ (0.1 mL). This mixture was loaded onto a BAKERBOND SPE^{TM} C18 cartridge (J.T.Baker, catalog number 7020-06, 6 mL, 500 mg). The cartridge was rinsed with water and then the desired product was eluted with ethanol to provide ((P)-1-(3-chloro-2-fluoro-5,5-dimethoxy-[1,1-biphenyl]-4-yl)-N-(isoxazol-3-yl)-2-oxo-1,2-dihydroquinoline-6-sulfonamide [5-methoxy-C^3H_3]) as a white solid: [185 MBq (5.0 mCi), 37 MBq (1.0 mCi) in EtOH]. Radioligand 4 corresponds to tritiated compound 501 and intermediate 3 corresponds to 'Intermediate BN' from (Weiss et al., 2014)

PatchXpress 7000A Electrophysiology. Sodium currents were recorded in whole cell voltage clamp mode with the PatchXpress automated electrophysiology system (Molecular Devices, LLC, Sunnyvale, CA). Adherent cells were isolated from tissue culture flasks using trypsin-EDTA treatment for 2-3 min and then incubated in complete culture medium containing 10% fetal bovine serum for at least 15 min prior to resuspension in external solution consisting of 70 mM NaCl, 140 mM D-Mannitol, 5 mM KCl, 11 mM Glucose, 10 mM HEPES, 2 mM $CaCl_2$, 1 mM $MgCl_2$, pH 7.4 with NaOH. Internal solution consisted of 62.5 mM CsCl, 75 mM CsF, 10 HEPES, 5 mM EGTA, 2.5 mM $MgCl_2$, pH 7.25 with CsOH. Cells were voltage clamped at room temperature at a holding potential of -125 mV with test potentials to -10 mV ($Na_V1.7$) or -20 mV ($Na_V1.5$). Compound effects were measured on a partially inactivated state of sodium channels.

JPET Fast Forward. Published on May 4, 2017 as DOI: 10.1124/jpet.116.239590
This article has not been copyedited and formatted. The final version may differ from this version.

For human, mouse, and rat $Na_V1.7$, cells were clamped to a holding potential yielding 20-50% inactivation. To elicit sodium current, channels were activated by pulsing to -10 mV for 15 msec. This voltage protocol was repeated at a rate of 0.1 Hz throughout the experiment. To evaluate AMG8379 inhibition of human $Na_V1.7$ in the closed/resting state, cells were clamped to a holding potential of -125 mV and activated by pulsing to -10 mV for 15 msec. For human $Na_V1.5$, cells were held at a holding potential of -50 mV. To elicit sodium currents the voltage was changed to -120 mV for a period of 50 msec before a test pulse to -20 mV of 20 msec duration. These voltage protocols were repeated at a rate of 0.1 Hz throughout the experiment. A single concentration of test compound was applied to cells for 3-5 min. Peak sodium current was measured at the end of the compound addition period to determine percent inhibition. Cells were used for additional compound testing if currents recovered to >80% of starting values following compound washout. IC_{50} values were calculated by pooling single point determinations from three to five cells at different compound concentrations and fitting the resulting dataset with a Hill (4-parameter logistic) fit in DataXpress 2.0 software.

IonWorks Quattro Electrophysiology. Sodium currents were recorded in population patch clamp mode with the IonWorks® Quattro automated electrophysiology system using the PatchPlate™ PPC population recording substrate (Molecular Devices, LLC, Sunnyvale, CA). This system utilizes perforated patch clamp technology to gain electrical access to cells. For assay, cells were grown to 60-90% confluency and lifted for 3 min at 37°C with either 0.25% Trypsin-EDTA (Gibco Life Technologies) for Na_V 1.1, 1.4, 1.5, 1.6 and 1.7 or TrypLE Express (Gibco Life Technologies) for $Na_V1.2$ and

JPET Fast Forward. Published on May 4, 2017 as DOI: 10.1124/jpet.116.239590
This article has not been copyedited and formatted. The final version may differ from this version.

$Na_V1.3$. Growth media was then added to the flasks and the cells were lightly triturated and then spun down for 3 min at 230xg. Cells were resuspended in external physiological saline (see below) at 2.5 million cells/ml for assay.

External saline consisted of (in mM): NaCl 140, KCl 5, $CaCl_2$ 2 $MgCl_2$ 1, HEPES 10 and glucose 11; pH 7.4 with N-methyl-D-glucamine; 320 mOsmol. Internal solution for $Na_V1.1$, 1.4, 1.5, 1.6 and 1.7 consisted of (in mM): of KCl 70, KF 70, $MgCl_2$ 0.25, HEDTA 5 and HEPES 10; pH 7.25 with N-methyl-D-glucamine; 300 mOsmol. We found that $Na_V1.2$ and $Na_V1.3$ currents were unstable with fluoride based internal solution and switched to a potassium gluconate based solution, which improved results. The internal solution used for $Na_V1.2$ and $Na_V1.3$ consisted of (in mM): K gluconate 100, KCl 30, $MgCl_2$ 3.2, EGTA 5 and HEPES 5; pH 7.25 N-methyl-D-glucamine; 300 mOsmol. Cell access was obtained using amphotericin (Sigma-Aldrich, St. Louis, MO) solubilized by sonication in DMSO (5mg/180 μl) and then diluted into 50 ml of internal saline, which was then introduced into the plenum on the intracellular side.

Cells were voltage clamped to -110 mV for three seconds (all Na_V channels except $Na_V1.5$) or half a second ($Na_V1.5$) and sodium currents were elicited by a train of 26 depolarizations of 150 msec duration at 5 Hz to -20 mV ($Na_V1.1$, 1.4, 1.5, 1.6 and 1.7) or to 0 mV ($Na_V1.2$ and 1.3) at a frequency of 5 Hz. Cells were then left unclamped for a period of 3 to 8 minutes while a single concentration of test compound was added. Following this compound incubation period, cells were then reclamped to -110 mV for three seconds (all Na_V channels except $Na_V1.5$) or half a second ($Na_V1.5$) to recover unbound channels and put through the same 26 pulse voltage protocol as above. Peak inward current during the 26th pulse to -20 mV or 0 mV in the presence of compound

JPET Fast Forward. Published on May 4, 2017 as DOI: 10.1124/jpet.116.239590
This article has not been copyedited and formatted. The final version may differ from this version.

was divided by the peak inward current evoked by the 26th pulse to -20 mV or 0 mV in the absence of compound to determine percent inhibition. Concentration-response curves of percent inhibition as a function of concentration were generated to calculate IC_{50} values. For IC_{50} determination, data was fitted to a 4-parameter equation (y = A + ((B-A)/(1 + ((x/C)^D))), where A is the minimum y (POC) value, B is the maximum y (POC), C is the x (compound concentration) at the point of inflection and D is the slope factor). Non-linear regression curve fitting was performed using Screener (Genedata AG, Basel, Switzerland) data analysis software.

DRG Neuron Isolation. Adult male and female C57BL/6 mice (Charles River Laboratories, San Diego, CA) were euthanized with CO_2 followed by decapitation. DRG from cervical, thoracic and lumbar regions were removed, placed in Ca^{2+} and Mg^{2+}-free Hanks' Balanced Salt Solution (Invitrogen, Carlsbad, CA), and trimmed of attached fibers under a dissecting microscope. DRG were sequentially digested at 37°C with papain (20 U/ml papain and 25 µM L-cysteine included, Worthington Biochemical Corporation, Lakewood, NJ) and in Ca^{2+} and Mg^{2+}-free Hanks' (pH 7.4) for 20-30 min and then with collagenase type 2 (0.3% w/v, Worthington Biochemical Corporation) for 20-30 min. Digestions were quenched with a 1:1 mixture of DMEM and Ham's F-12 Nutrient Mixture (Invitrogen) supplemented with 10% calf serum (Invitrogen), and cells were triturated with a fire-polished Pasteur pipette prior to plating on Poly-D-Lysine-coated glass coverslips (Cole-Parmer, Vernon Hills, IL). Cells were maintained in a humidified incubator at 32°C with 5% CO_2 for 3-7 days in the presence of 2% B27

Supplement (Thermo Fisher Scientific) to increase the expression of tetrodotoxin-sensitive sodium channel currents.

Manual Patch Clamp Electrophysiology. DRG neurons (20-30 μm diameter) were voltage clamped using the whole-cell patch clamp configuration at room temperature (21-24ºC) using an Axopatch 200 B or MultiClamp 700 B amplifier and DIGIDATA 1322A with pCLAMP software (Molecular Devices, Sunnyvale, CA). Pipettes, pulled from borosilicate glass capillaries (World Precision Instruments, Sarasota, FL), had resistances between 1.0 and 3.0 MΩ. Voltage errors were minimized using >80% series resistance compensation. A P/4 protocol was used for leak subtraction. Voltages were uncorrected for liquid junction potentials. Currents were digitized at 50 kHz and filtered (4-pole Bessel) at 10 kHz. Cells were lifted off the culture dish and positioned directly in front of a micropipette connected to a solution exchange manifold for compound perfusion. Cells were held at a voltage yielding approximately 20% inactivation and depolarized to -10 mV for 40 msec every 10 seconds. Pipette solution contained (in mM): 62.5 CsCl, 75 CsF, 2.5 $MgCl_2$, 5 EGTA, and 10 HEPES, pH 7.25 by CsOH. Bath solution contained (in mM): 70 NaCl, 5.0 KCl, 2.0 $CaCl_2$, 1.0 $MgCl_2$, 10 HEPES, and 11 glucose, 140 mannitol, pH 7.4 by NaOH. U-2 OS cells transduced with mouse $Na_V1.1$ or mouse $Na_V1.6$ BacMam viruses and human $Na_V1.2$ CHO cells were evaluated using a voltage protocol that mimics the IonWorks Quattro protocol as previously described (Figure 11D in (Liu et al., 2016)) in which cells are clamped to -20 mV to mimic the unclamped state during compound addition and incubation. For U-2 OS and CHO cells, pipette solution contained (in mM): 62.5 CsCl, 75 CsF, 2.5 $MgCl_2$, 5

JPET Fast Forward. Published on May 4, 2017 as DOI: 10.1124/jpet.116.239590
This article has not been copyedited and formatted. The final version may differ from this version.

EGTA, and 10 HEPES, pH 7.25 by CsOH. Bath solution contained (in mM): 140 NaCl, 5.0 KCl, 2.0 $CaCl_2$, 1.0 $MgCl_2$, 10 HEPES, and 11 glucose, pH 7.4 by NaOH. Data were analyzed with Clampfit and Origin Pro8 (OriginLab Corp, Northampton, MA).

Skin-Nerve Preparation. Methods for isolating and recording from the saphenous nerve-skin preparation were modified from those previously described (Lennertz et al., 2012; Gingras et al., 2014). Briefly, the saphenous nerve and skin from the medial dorsum of the hindpaw of 2-3 month old male C57BL/6 mice were rapidly dissected from the left leg. The entire skin nerve preparation was removed and mounted in a custom made organ bath chamber (CT Tool company, Inc, Mountain View, CA, USA) with corium side up. The bath was superfused at 15 ml/min with 30°C and oxygen-saturated synthetic interstitial fluid containing the following (in mM): 123 NaCl, 4 KCl, 0.7 $MgSO_4$, 1 NaH_2PO_4, 2.0 $CaCl_2$, 9.5 sodium gluconate, 10 glucose, 7.5 sucrose, and 10 HEPES, osmolarity 295 mOsm, pH 7.40 adjusted with NaOH. The proximal end of the saphenous nerve was passed through a hole into a separate, mineral-oil-filled recording chamber, desheathed, and teased into fine fibers for extracellular recordings. Single fiber receptive fields in skin were detected by light pressure with a blunt glass rod. Fiber type was determined by action potential conductance velocity following receptive field electrical stimulation with square wave pulses (0.3-0.5 ms; 4-6 mA) delivered through a stainless steel microelectrode. Fibers with a conduction velocity less than 1.2 m/s were classified as C-fibers.

Mechanical responses were evoked by square waves of force using a mechanical stimulator (Dual-Mode Lever Systems, Aurora Scientific Inc., Canada) in ascending order of 1, 50, 100, 150 and 200 mN (10 seconds per pulse with 300 second inter-stimulus intervals) or a constant stimulation force of 150 mN (10 seconds per pulse with 300 second inter-stimulus intervals). Thermal responses were evoked by perfusion of synthetic interstitial fluid solution through two heating systems connected in series (first heater from ThermoClamp, AutoMate Scientific, Berkeley, CA and second heater from Warner Instruments, Hamden, CT). Thermal stimuli were applied in ascending order from 30, 33, 38, 43 to 48°C (10 seconds per pulse with 300 seconds inter-stimulus intervals) or using a constant thermal pulse (48°C, 10 seconds per pulse with 300 seconds inter-stimulus intervals).

All compounds were directly applied to a small area of the corium (dermis) side of the skin in a custom-made stainless steel ring (5 mm diameter, 12 mm high; CK Tool Company, Inc.). Two mechanical or two thermal stimuli were applied before compound treatment and the average firing frequency from these pulses was used for the baseline. To identify fiber types as TTX-sensitive or TTX-resistant, 1 μM Tetrodotoxin (TTX; Sigma) or 1 μM of the $Na_V1.8$ blocker (compound 31 from (Kort et al., 2010)) were applied at the end of each recording. Fibers were classified as TTX-sensitive if TTX blocked over 90% of induced action potentials and fibers were classified at TTX-resistant if TTX blocked less than 90% of induced action potentials. Signals were recorded by a Neurolog system (Digitimer, UK) and Spike 2 software (Cambridge Electronic Design Ltd, UK). Action potentials were discriminated and counted using

spike histogram software in Spike 2. Stimulus-evoked action potentials were determined by subtracting the spontaneous firing rate from the mechanical or thermal-evoked firing rate. Both recordings and analyses were performed in a blind manner with respect to compound treatment. All data were analyzed by Graph Pad Prism 6 (Graph Pad Software, La Jolla, CA) and OrigenPro 2016 (Origen Lab, Northampton, MA).

Determination of Unbound Fraction in Plasma. The unbound fraction (f_u) of AMG8379 and AMG8380 was determined in mouse plasma (pooled, mixed-gender conducted in triplicate). Each compound was dissolved in DMSO and spiked into plasma at a final concentration of 5 µM. The resulting plasma samples were subject to ultracentrifugation and liquid chromatography-mass spectrometry analysis as described previously (DiMauro et al., 2016). AMG8379, AMG8380 and a proprietary internal standard were monitored in positive ionization mode at multiple reaction monitoring transitions of 544.1 / 397.2 (Q1/Q3; AMG8379 and AMG8380) and 455.1 / 318.2 (Q1/Q3; internal standard), respectively. The concentration of each compound was calculated by comparing the peak areas of the test samples to those from synthetic standard curves (linear range = 0.003 – 100 µg/mL). The f_u values were derived as a ratio of the compound concentration in the supernatant from the ultracentrifugation samples versus the concentration in plasma samples that were stored at 4°C for the duration of the experiment.

Mouse Pharmacokinetic and Pharmacodynamic Analyses. To determine the pharmacokinetic properties of AMG8379 after oral administration, the compound was

JPET Fast Forward. Published on May 4, 2017 as DOI: 10.1124/jpet.116.239590
This article has not been copyedited and formatted. The final version may differ from this version.

formulated in 2-hydroxypropyl-β-cyclodextrin/water (30:70 v/v; pH 10.0) and dosed at either 10, 30 or 100 mg/kg to 8-10 week old male C57BL/6 or CD-1 mice (Charles River, Wilmington, MA). Blood samples were collected and placed in K_2-EDTA plasma collection tubes prior to centrifugation at 13,000 rpm for 10-15 minutes. The preparation of the plasma samples was similar to that described for the ultracentrifugation assay, except that 5 volumes (v/v) of ice cold acetonitrile was utilized to precipitate plasma proteins prior to mass spectrometry analysis. Plasma samples from pharmacodynamic assays were prepared in an identical manner to the pharmacokinetic samples. Non-compartmental analysis was used to calculate the pharmacokinetic parameters following oral administration (Phoenix64, Cetara, Princeton, NJ).

For measurement of brain concentrations, mice were euthanized via exposure to carbon dioxide followed by collection of brain tissue. The collected brains were homogenized using four volumes of water (v/v) containing 0.1% formic acid. Appropriate standard curves were prepared using control brain tissue from untreated mice. Six volumes of ice-cold acetonitrile containing a proprietary internal standard were added to aliquots of homogenate (test samples and standard curve). All samples were vortex-mixed and centrifuged at 3,000 rpm for 15 minutes. A portion of the resulting supernatant was added to an equal volume of 0.1% formic acid in water prior to analysis by mass spectrometry as described above. Brain:plasma ratios were calculated by comparing the absolute concentrations of the compounds in each matrix.

Behavioral Experiments. In all studies, experimental procedures were approved by Amgen Inc.'s Institutional Animal Care and Use Committee in accordance with the National Institutes of Health's Guide for the Care and Use of Laboratory Animals and conducted at an AALAC-accredited facility. Subjects were either C57Bl/6 or CD-1 male mice (Charles River Laboratories, Franklin, NY and San Diego, CA) aged between 8-10 weeks at the beginning of each study. Animals were kept under standard temperature conditions (22–24°C) and illumination (12-hour light/dark cycle with lights on at 6:30 AM). They were allowed to adjust to this environment for at least 7 days in solid-bottom cages before the experiments began and were given *ad libitum* access to fresh water and food. In all studies, blood samples were collected immediately after behavioral testing for pharmacokinetic analyses. Statistical analysis of behavioral data was performed via GraphPad Prism 5 software (GraphPad Software Inc., La Jolla, CA) using a one-way ANOVA to test for a drug-treatment effect and followed by Dunnett's multiple comparison post-hoc tests.

Open-Field Locomotor Activity in Mice. On the day of testing, C57Bl/6 male mice were orally administered either AMG8379 (10, 30, or 100 mg/kg body weight) or a vehicle control formulation (2-hydroxypropyl-β-cyclodextrin/water (30:70 v/v; pH 10.0)) at a dose volume of 10 ml/kg. Four hours following test article treatment, animals were placed into dimly-lit open-field chambers (16" x 16", Kinder Scientific, San Diego, CA) and behavior was monitored over a 30 minute period during which locomotor activity (horizontal movement) parameters were measured in an automated manner via infrared photo-beam breaks.

JPET Fast Forward. Published on May 4, 2017 as DOI: 10.1124/jpet.116.239590
This article has not been copyedited and formatted. The final version may differ from this version.

Histamine-Induced Scratching in Mice. One day prior to behavioral testing, C57Bl/6 male mice were anesthetized under 3% isoflurane and the area at the nape of the neck was shaved. Immediately afterward, mice were transported to the testing room and acclimated to individual sound-attenuated chambers (12”l X 9.5”w X 8.25”h, Med Associates VFC-008, NIR-022MD, St. Albans, VT) for 15-20 minutes. Testing was performed the following day between the hours of 8:00 AM and 3:00 PM. Four hours prior to histamine treatment, mice were orally administered either AMG8379 (10, 30, or 100 mg/kg body weight), AMG8380 (100 mg/kg), or a vehicle control formulation (2-hydroxypropyl-β-cyclodextrin/water (30:70 v/v; pH 10.0)). A separate group of animals was orally administered the antihistamine diphenhydramine (30 mg/kg in phosphate-buffered saline; Sigma D3630) 90 minutes prior to testing to serve as a positive control. Histamine dichloride (8.15 mM in a volume of 100 µL; Sigma, H7250) was injected intradermally to the shaved area, mice were placed into the sound-attenuated testing chambers, and behavior was recorded on digital video files for a period of 15 minutes. Video recordings were later reviewed and individual scratching bouts were scored by trained experimenters. A scratching bout was defined as a rapid head tilt accompanied by a hind paw directed at the site of intradermal injection. Termination of a scratching bout was deemed to have occurred when the hind paw was placed back on the chamber floor or into the animal’s mouth. All dosing and scoring activities were conducted by experimenters who were fully blinded to treatment conditions.

UVB-Induced Thermal Hyperalgesia in Mice. Two days prior to thermal sensitivity testing, C57Bl/6 male mice were habituated for two hours to the plantar test equipment (IITC, Woodland Hills, CA) and their testing chambers. Mice were placed in a Perspex cylinder 4" in diameter and 5" high atop the glass IITC testing surface, with the surface temperature set to 30ºC. Holes were drilled into the sides and top of the testing chamber to allow for adequate airflow. After habituation, mice were subject to UV irradiation. Specifically, animals were gently restrained in a cloth glove with the left plantar hind paw exposed. The area just proximal to the foot pads was treated with 200 mJ/cm^2 of UV irradiation with the MEDlight CUP-CUBE system (Herford, Germany). Animals were then returned to their home cages overnight. One day prior to thermal sensitivity testing, animals were once again habituated to the IITC apparatus and testing chambers for three hours and then returned to their home cages overnight. On test day, animals were placed in the testing chambers and allowed to acclimate until calm, typically for 90 minutes. Thermal threshold baseline measurements were then taken on the contralateral (non-irradiated, uninjured) and ipsilateral (irradiated, injured) hind paw with the IITC heat source set to an intensity level of AI = 19. This intensity was previously calibrated to elicit an average paw withdrawal latency of 17 seconds in a non-irradiated animal. The contralateral paw withdrawal latency was always assessed first, followed by measurement of paw withdrawal latency on the ipsilateral side. Thermal hypersensitivity was assessed using a method slightly modified from that described previously (Hargreaves et al., 1988). Briefly, the heat source was positioned under the mouse hind paw just proximal to the paw pads. Once the heat source was turned on, the latency for the animal to remove its hind paw from the stimulus was

JPET Fast Forward. Published on May 4, 2017 as DOI: 10.1124/jpet.116.239590
This article has not been copyedited and formatted. The final version may differ from this version.

recorded as a trial. Two trials were taken per paw with an inter-trial interval of at least 10 minutes. If the two trials were not within 5 seconds of each other, a third measurement was taken. An automatic cut-off latency of 30 seconds was applied to prevent tissue damage. The baseline score for each paw was defined as the average paw withdrawal latency (in seconds) taken by the mouse to remove its hind paw from the heat source. After baseline measurements, mice were randomized into groups by the difference score between both paws and dosed orally with AMG8379 (10, 30, or 100 mg/kg), AMG8380 (100 mg/kg), naproxen (30 mg/kg), or 2-hydroxypropyl-β-cyclodextrin/water (30:70 v/v; pH 10.0 with NaOH) vehicle. All dose groups had a four hour pretreatment time, except the naproxen group, which had a two hour pretreatment time. During the first two hours following compound administration, animals were placed back into their home cages and allowed access to food and water. Immediately following the dosing of the naproxen group, all animals were transferred to the testing chambers and allowed to reacclimatize to the testing environment. Once the pretreatment time had elapsed, the irradiated hind paw was tested as stated above. All dosing and scoring activities were conducted by experimenters who were fully blinded to treatment conditions.

Capsaicin-Induced Nociception in Mice. On the day of testing, CD-1 male mice were orally administered either AMG8379 (30 or 100 mg/kg body weight), a vehicle control formulation (2-hydroxypropyl-β-cyclodextrin/water (30:70 v/v; pH 10.0)) or a positive control in the form of the potent TRPV1 antagonist AMG 517 (Doherty et al., 2007). Four hours following test article treatment (1.5 hours for AMG 517), animals were

JPET Fast Forward. Published on May 4, 2017 as DOI: 10.1124/jpet.116.239590
This article has not been copyedited and formatted. The final version may differ from this version.

subject to intraplantar injection of 1 ug of capsaicin (Sigma, M2028-50MG) in a volume of 20 µl of 10% EtOH/1% Tween-80 in phosphate-buffered saline without Ca^{2+} and Mg^{2+} (Sigma) into the left hind paw. Immediately after the capsaicin injection, the total time spent engaged in licking of the injected hind paw was manually recorded over a 5 minute period. All dosing and scoring activities were conducted by experimenters who were fully blinded to treatment conditions.

Results

AMG8379 Antagonist Activity. AMG8379 and AMG8380 represent a pair of atropisomeric quinolone sulfonamides discovered in our efforts to identify an isoform-selective $Na_V1.7$ inhibitor (Fig. 1A). Discovery and optimization of drug-like properties for this chemical class is described in a separate report (Graceffa et al., 2017). AMG8379 potently inhibited recombinant human and mouse, but not rat, $Na_V1.7$ channels expressed in heterologous HEK293 cells when evaluated by automated patch clamp electrophysiology on a PatchXpress 7000A system using a voltage protocol where 20-50% of channels were in an inactive state (Table 1, Supplemental Figure 1). By contrast, AMG8380 was over one hundred-fold less potent on human $Na_V1.7$ and over twenty-fold less potent on mouse $Na_V1.7$ (Table 1, Supplemental Figure 1). AMG8379 inhibition of human $Na_V1.7$ was state-dependent as potency values decreased over 60-fold when evaluated on channels in the closed/resting state (Table 1). When evaluated in mouse DRG neurons expressing endogenous $Na_V1.7$ using manual patch clamp electrophysiology, AMG8379 potently and reversibly blocked TTX-sensitive native channels with an IC_{50} of 3.1 ± 0.1 nM (mean ± SEM; n=6) whereas AMG8380 was nearly one thousand-fold less potent with an IC_{50} of 2,560 ± 743 nM (n=4) (Table 1, Fig. 1B-C). Neither AMG8379 nor AMG8380 blocked TTX-resistant channels (representing native $Na_V1.8$ currents) in mouse DRG neurons when tested up to 5 μM (Fig. 1D). AMG8379 was over one hundred to one thousand-fold selective against other human and mouse Na_V isoforms expressed in heterologous cells when evaluated by automated patch clamp electrophysiology on an IonWorks Quattro system using a 5 Hz use-dependent voltage protocol where channels are repetitively cycled

JPET Fast Forward. Published on May 4, 2017 as DOI: 10.1124/jpet.116.239590
This article has not been copyedited and formatted. The final version may differ from this version.

through closed, open, and inactive states (Table 2, Supplementary Figure 2). Using a radioligand binding assay that interrogates compound interaction with the fourth voltage-sensor domain of the human $Na_V1.7$ channel in HEK293 membranes, AMG8379 displaced a tritiated heteroaryl sulfonamide with a K_i of 3.7 ± 1.0 nM, similar to the IC_{50} value determined by electrophysiology, whereas AMG8380 displaced the label with a K_i of 167.1 ± 74.3 nM. Thus, AMG8379 and AMG8380 represent an active and much less active pair of atropisomers that bind to the fourth voltage-sensor domain of $Na_V1.7$ and can be utilized to evaluate the role of $Na_V1.7$ in specific pharmacological endpoints.

Inhibition of Mechanically-Induced Action Potential Firing by AMG8379.

Mechanical stimulation of afferent nerve terminals resulted in a force-dependent increase in C-fiber action potential firing in a mouse skin-saphenous nerve preparation (Fig.2A). Near maximal firing frequencies were obtained when receptive fields were stimulated with 150mN mechanical forces (10.0 ± 1.4 Hz; n=25; Fig. 2B; similar to the firing frequencies previously reported (Koltzenburg et al., 1997; Hoffmann et al., 2008)); therefore, 150 mN was chosen as the mechanical stimulus for subsequent experiments with AMG8379 and AMG8380. TTX applied to the receptive field in the skin at a concentration of 1 μM robustly blocked mechanically-stimulated C-fiber firing (Fig. 2B; repeated measures two-way ANOVA, $F(1, 48) = 33.2$, $P < 0.0001$), and TTX dose-dependently blocked C-fiber spiking with an IC_{50} of 15.7 ± 0.9 nM (Fig. 2C-D).

AMG8379 applied to afferent nerve terminals dose-dependently decreased mechanically-induced C-fiber action potential firing compared to 0.1% DMSO vehicle control (Fig. 3A-B; repeated measures two-way ANOVA, $F(3, 81) = 7.7$, $P = 0.0001$).

Previously, we reported that mechanically-induced C-fiber action potential firing in response to a 150 mN stimulus in $Na_V1.7$ knockout mice was reduced to approximately 40% of wild-type levels (Gingras et al., 2014). A similar reduction was observed with 700 nM AMG8379 after 25 minutes (normalized firing frequency of 44.3 ± 9.6%; Fig. 3B). Therefore, we calculated the IC_{50} for AMG8379 inhibition of C-fiber spiking based on the level of firing in $Na_V1.7$ KO mice representing complete pharmacological block of the $Na_V1.7$-component of this assay. In this manner, the IC_{50} for AMG8379 block was 47.0 ± 8.1 nM (Fig. 3C). When evaluated at 470 nM, the less active enantiomer AMG8380 had a nominal effect on mechanically-induced C-fiber spiking whereas the same concentration of the active enantiomer AMG8379 blocked C-fiber spiking (Fig. 4A-B; repeated measures two-way ANOVA, $F(1, 44) = 13.1$, $P = 0.0007$). These data indicate that AMG8379 inhibition of $Na_V1.7$ channels in afferent nerve terminals blocks mechanically-induced action potential firing in C-fibers.

Inhibition of Thermally-Induced Action Potential Firing by AMG8379. Thermal stimulation of afferent nerve terminals resulted in a temperature-dependent increase in C-fiber action potential firing in a mouse skin-saphenous nerve preparation (Fig.5A). Near maximal firing frequencies were obtained when receptive fields were stimulated with 48^{o}C (2.1 ± 0.2 Hz after 25 minutes; n=8; Fig. 5B; similar to the firing frequencies previously reported (Kwan et al., 2009)); therefore, 48^{o}C was chosen as the thermal stimulus for subsequent experiments with AMG8379 and AMG8380. AMG8379 applied to afferent nerve terminals at a concentration of 470 nM significantly decreased thermally-induced C-fiber action potential firing compared to 470 nM AMG8380 (Fig. 6A-

JPET Fast Forward. Published on May 4, 2017 as DOI: 10.1124/jpet.116.239590
This article has not been copyedited and formatted. The final version may differ from this version.

B; repeated measures two-way ANOVA, F(1, 30) = 6.0, P = 0.02). TTX applied to the receptive field in the skin at a concentration of 1 μM completely blocked thermal-stimulated C-fiber firing in these fibers (normalized firing frequency of 0.9 ± 0.3% after 25 minutes; n=32; Fig. 6A). Thermal stimulation of a subset of C-fibers was not robustly blocked by 1 μM TTX application. In these TTX-resistant fibers, 470 nM of either AMG8379 or AMG8380 had no significant differential effect on thermally-induced action potential firing (Fig. 7A-B; repeated measures two-way ANOVA, F(1, 25) = 0.7, P = 0.3997). By contrast, 1 μM of a $Na_V1.8$ selective blocker robustly suppressed thermal responses (normalized firing frequency of 4.6 ± 2.1% after 25 minutes; n=13; Fig. 7A). These data indicate that AMG8379 inhibition of $Na_V1.7$ channels in afferent nerve terminals blocks thermally-induced action potential firing in TTX-sensitive C-fibers but not TTX-resistant C-fibers.

AMG8379 Does Not Affect Locomotor Activity in Mice. Following oral dosing up to 100 mg/kg, AMG8379 was restricted to the periphery with a brain-to-plasma ratio of 0.01. To evaluate if behavioral measurements of itch and pain in pharmacodynamic models could be confounded by non-specific impairments of sensorimotor function, locomotor activity was monitored following oral dosing of AMG8379. As shown in Fig. 8, there was no statistically significant difference between vehicle and AMG8379 cohorts in total activity as assessed by beam breaks in an open-field arena over the 30 minute test session [one-way ANOVA, F(3, 36) = 0.06, P = 0.98]. Thus, AMG8379 showed no evidence of adversely impacting locomotor activity, allowing for reliable and

JPET Fast Forward. Published on May 4, 2017 as DOI: 10.1124/jpet.116.239590
This article has not been copyedited and formatted. The final version may differ from this version.

specific assessment of its effects on itch- and pain-related behaviors in mice at doses up to 100 mg/kg.

Inhibition of Histamine-Induced Scratching by AMG8379. Intradermal application of histamine led to demonstrable scratching behavior in mice at the site of injection that persisted over a 15 minute test period. This response could be prevented by pretreatment with a 30 mg/kg dose of the antihistamine diphenhydramine. Oral administration of AMG8379 dose-dependently blocked histamine-induced scratching behavior, with a minimal effective dose of 30 mg/kg and with a 100 mg/kg dose yielding near-complete elimination of scratching bouts [Fig. 9A, one-way ANOVA, $F(4, 43) = 39.7$, $P < 0.0001$]. By contrast, the less active enantiomer AMG8380 failed to show a statistically significant effect on scratching behavior at equivalent doses and plasma exposures to AMG8379, whereas, once again AMG8379 produced a robust and statistically significant reduction in scratching bouts at a dose of 100 mg/kg [Fig. 9B and Table 3, One-way ANOVA, $F(4, 42) = 8.0$, $P < 0.001$; Dunnett's post hoc tests for AMG8380, $p > 0.05$ for all doses and $p < 0.001$ for AMG8379 compared to vehicle group].

Inhibition of UVB-Induced Thermal Hyperalgesia by AMG8379. UVB irradiation to the plantar surface of the hind paw caused thermal hyperalgesia in mice when assessed 48 hours after induction of the burn injury, as illustrated by the robust decrease in paw withdrawal latency in response to a mildly noxious heat stimulus

JPET Fast Forward. Published on May 4, 2017 as DOI: 10.1124/jpet.116.239590
This article has not been copyedited and formatted. The final version may differ from this version.

applied to the injured (ipsilateral) paw compared to the non-injured (contralateral) paw (Fig 10A). When animals were pretreated with the anti-inflammatory agent naproxen (30 mg/kg), thermal hypersensitivity was completely reversed with the mean withdrawal latency returning to the level associated with the non-irradiated contralateral paw. Oral administration of AMG8379 at a dose of 100 mg/kg led to an analgesic effect similar to that observed with naproxen [Fig 10A, one-way ANOVA, $F(5, 56) = 6.8$, $P < 0.0001$], and the mean paw withdrawal latency of the ipsilateral side was not significantly different from the contralateral side. Lower doses of AMG8379 (10 and 30 mg/kg) had no significant effect on UVB-induced thermal hyperalgesia. When administered at a dose of 100 mg/kg, the less active enantiomer AMG8380 did not impact paw withdrawal latencies at similar plasma exposures to those achieved with 100 mg/kg of AMG8379 (Fig 10A and Table 3).

Inhibition of Capsaicin-Induced Nociceptive Behavior by AMG8379. Intradermal application of the TRPV1 agonist capsaicin produced a robust nociceptive response in mice as evidenced by hind paw lifting and licking behavior that persisted over the 5 minute observation period. The potent and selective TRPV1 antagonist AMG 517 (Doherty et al., 2007) effectively blocked the capsaicin-elicited response. AMG8379 showed a dose-dependent reduction in overall nociceptive behavior, with a 100 mg/kg oral dose leading to a statistically significant reduction in total time engaged in paw licking [Figure 10B, one-way ANOVA, $F(3, 34) = 16.6$, $P < 0.0001$]. Plasma concentration of AMG8379 at 100 mg/kg was comparable to that observed in both the histamine-induced scratch and UVB-induced thermal hyperalgesia studies (Table 3).

Discussion

AMG8379 is a potent and selective small molecule sulfonamide antagonist of human and mouse, but not rat, recombinant $Na_V1.7$ channels in heterologous cells and native $Na_V1.7$ channels in mouse DRG neurons. AMG8379 inhibited mechanically- and thermally-induced C-fiber action potential firing in a mouse skin-nerve preparation and blocked multiple $Na_V1.7$-dependent behaviors including histamine-induced scratching, capsaicin-induced licking, and UVB-induced thermal hyperalgesia. The significantly less active atropisomer AMG8380 did not affect behavioral endpoints, pointing to a specific requirement for $Na_V1.7$ target engagement to achieve these effects. We believe this represents the first report describing the pharmacological characterization of an active and less active $Na_V1.7$ enantiomeric pair in a battery of *in vitro*, *ex vivo*, and *in vivo* experiments.

When applied to the dermal side of the skin, AMG8379 reduced C-fiber action potential firing following both mechanical and thermal stimulation of receptive fields in *ex vivo* mouse skin-nerve preparation experiments. Nominal inhibition was observed with the less active atropisomer AMG8380, pointing to specific block of $Na_V1.7$ accounting for these observations. $Na_V1.7$ is expressed in dermal nerve fibers in human skin as well as dermal and epidermal nerve terminals in rodent skin (Black et al., 2012; Rice et al., 2015). We propose that engagement of $Na_V1.7$ in skin nerve fibers by AMG8379 attenuates mechanically- and thermally-induced action potential firing. Notably, the degree of C-fiber action potential firing inhibition observed with the highest concentration of AMG8379 tested (700 nM) was similar to the residual level of C-fiber activity in preparations from $Na_V1.7$ knockout mice following mechanical stimulation

(Gingras et al., 2014). Defining the level of C-fiber activity in $Na_V1.7$ KO mice as the maximal level of $Na_V1.7$ pharmacological block obtained in the *ex vivo* skin-nerve preparation, the IC_{50} for AMG8379 inhibition of mechanically-induced action potential firing was 47 nM, or 2.5-fold the m$Na_V1.7$ IC_{50} (compared to the potency on partially-inactivated channels as measured on the PatchXpress platform), and near full block was observed at 700 nM AMG8379 or 38-fold the m$Na_V1.7$ IC_{50}. Higher concentrations of AMG8379 required to block action potential firing in nerve fibers compared to Na_V current in cultured DRG neurons or heterologous cells could be due to dermal tissue barriers that preclude compound access to $Na_V1.7$ channels in the skin-nerve preparation and/or a requirement for few available channels in a high-resistance nerve membrane to depolarize the membrane potential to the threshold for action potential firing. AMG8379 effects were maximal following 25 min of incubation, consistent with slow diffusion through tissue and similar to a previous report in which lower concentrations of TTX required 30-40 min to block nerve conduction (Pinto et al., 2008). In hippocampal neurons, 16-fold higher levels of TTX were required to block action potential firing compared to sodium currents (Madeja, 2000). High receptor occupancy of $Na_V1.7$ is likely required to robustly impact sensory neuron action potential firing. A small number of available $Na_V1.7$ channels would support inward sodium currents contributing to both sub-threshold ramp currents as well as the upstroke of nociceptor action potentials.

We did not evaluate higher concentrations of AMG8379 in skin-nerve studies, to determine if full block of C-fiber spiking could be achieved, in order to avoid potential inhibition of non-$Na_V1.7$ channels. Full block of mechanically- and thermally-induced C-

JPET Fast Forward. Published on May 4, 2017 as DOI: 10.1124/jpet.116.239590
This article has not been copyedited and formatted. The final version may differ from this version.

fiber spiking was obtained with TTX, indicating the presence of non-$Na_V1.7$ TTX-S channels in these fibers. In addition to $Na_V1.7$ expression in small diameter DRG neurons whose axons correspond to C-fibers (Fukuoka et al., 2008; Fukuoka and Noguchi, 2011; Ho and O'Leary, 2011; Theriault and Chahine, 2014), expression and function of $Na_V1.1$ and $Na_V1.6$ have been reported (Fukuoka et al., 2008; Zhang et al., 2013; Chiu et al., 2014; Usoskin et al., 2015). Given the lack of potent inhibition of mouse $Na_V1.1$ and mouse $Na_V1.6$ by AMG8379, we do not attribute inhibition of C-fiber activity to engagement of these channels. The IC_{50} for AMG3879 inhibition of mouse $Na_V1.1$ was >30 μM and the IC_{50} for AMG3879 inhibition of mouse $Na_V1.6$ was 2.74 μM; these values are above the highest concentrations of AMG3879 used in skin-nerve prep experiments (0.5-0.7 μM). The population of thermoresponsive C-fibers not blocked by TTX supports a critical role for TTX-resistant channels such as $Na_V1.8$ in mediating action potential firing in small diameter DRG neurons (Renganathan et al., 2001; Blair and Bean, 2002). In support of this, a $Na_V1.8$-specific small molecule antagonist, but not the $Na_V1.7$-specific antagonist AMG8379, blocked thermally-induced C-fiber spiking in TTX-resistant thermoresponsive C-fibers when tested at 1 uM, a concentration 36-fold higher than the reported IC_{50} of 28 nM on TTX-R currents in rat DRG neurons (Kort et al., 2010). We did not directly extend our analyses to A-delta or A-beta fibers, which also may express $Na_V1.7$ (Fukuoka and Noguchi, 2011; Ho and O'Leary, 2011).

The somatosensory modalities of pain and itch induce differential behavioral responses via activation of sensory ganglia neurons expressing machinery to detect nociceptive and pruritic stimuli (Basbaum et al., 2009; Davidson and Giesler, 2010; Liu and Ma, 2011; Bautista et al., 2014). Nociceptive stimuli lead to withdrawal behavior in

JPET Fast Forward. Published on May 4, 2017 as DOI: 10.1124/jpet.116.239590
This article has not been copyedited and formatted. The final version may differ from this version.

order to minimize tissue damage, whereas pruritic stimuli lead to scratching behavior in order to dislodge irritants. Histamine is a pruritogen that activates G protein-coupled receptors on primary afferents, increases intracellular calcium and activates TRPV1 channels that lead to depolarizing receptor potentials; capsaicin is an algogen that directly gates TRPV1 channels which lead to similar depolarizing receptor potentials (Davidson and Giesler, 2010). We propose that histamine- and capsaicin-induced receptor potentials activate $Na_V1.7$ leading to action potential initiation in primary afferent nerve fibers. We were unable to use either histamine or capsaicin as direct stimuli in skin-nerve preparation experiments due to poor responses to histamine when tested up to mM levels and desensitization of responses with capsaicin precluding repeated testing pre- and post-pharmacological challenge. The critical role of $Na_V1.7$ in histamine-induced itch is supported by abrogation of scratching responses following intradermal histamine injection in mice with genetic deletion of $Na_V1.7$ from birth (Gingras et al., 2014). In humans, a $Na_V1.7$ gain-of-function mutation that decreases slow inactivation is linked to paroxysmal itch and pain attacks following environmental warmth or consumption of spicy foods, further implicating TRPV1 upstream of $Na_V1.7$ activation (Devigili et al., 2014). In humans with loss-of-function $Na_V1.7$ congenital insensitivity to pain mutations, pain following capsaicin chemical challenge has not been reported, but would be anticipated to be deficient give loss of thermal pain in these individuals (Cox et al., 2006; Goldberg et al., 2007). The critical role of $Na_V1.7$ in capsaicin-induced pain behavior in mice is supported by loss of licking responses following intradermal capsaicin injection into mice with genetic deletion of $Na_V1.7$ from birth (unpublished data), which will be described in a subsequent report. Collectively,

JPET Fast Forward. Published on May 4, 2017 as DOI: 10.1124/jpet.116.239590
This article has not been copyedited and formatted. The final version may differ from this version.

these data suggest that $Na_V1.7$ is expressed on both nerve fibers dedicated to itch perception, including those responsive to histamine, as well as TRPV1-positive nerve fibers responsive to capsaicin, and that $Na_V1.7$ function is essential for orthodromic action potential transmission toward the spinal cord.

AMG8379, a peripherally-restricted molecule with nominal access to central compartments as reflected by the brain-to-plasma ratio of 0.01, robustly blocked multiple $Na_V1.7$-dependent behavioral endpoints. Specific inhibition of histamine-induced scratching and UVB-induced thermal hyperalgesia behavior by AMG8379 but not the less active atropisomer AMG8380 indicates that antagonism of $Na_V1.7$ in peripheral compartments is sufficient to block both itch and pain behavior in pre-clinical models. Robust inhibition of these behaviors in mice by AMG8379 was observed at circulating free drug plasma concentrations between 15- and 23-fold over the mouse $Na_V1.7$ IC_{50} (compared to the potency on partially-inactivated channels as measured on the PatchXpress platform). Importantly, at equivalent plasma exposure levels, AMG8379 did not result in any potentially confounding effects on locomotor activity in an open-field assessment. Moreover, a similar target coverage multiple was required to robustly block C-fiber action potential firing in the ex vivo skin-nerve preparation. Circulating free drug plasma concentrations of AMG8379 were only ~10% of the mouse $Na_V1.6$ IC_{50} value, arguing that mouse $Na_V1.6$ engagement would not account for the behavioral results observed in our pharmacodynamic studies. Notably, both the capsaicin and UVB pain models represent highly translatable models for clinical investigation with high predictability of analgesic drug development success (Oertel and Lotsch, 2013; Lotsch et al., 2014; Arendt-Nielsen et al., 2016).

Our findings are consistent with reports that poorly selective or $Na_V1.7$-prefering small molecule antagonists can block spontaneous or evoked pain responses in preclinical species (Brochu et al., 2006; Haroutounian et al., 2014; Matson et al., 2015; Alexandrou et al., 2016; Deuis et al., 2016; Focken et al., 2016; Frost et al., 2016; Hockley et al., 2017). Clinically, a small cohort of individuals with $Na_V1.7$ gain-of-function mutations causing inherited erythromelalgia exhibited lower pain scores in response to thermal challenge following acute dosing with a sulfonamide antagonist (Cao et al., 2016). A critical unanswered question in the field is whether a $Na_V1.7$-selective and CNS-penetrant blocker, that could engage channels not only on peripheral nerve fibers but also in central terminals of primary afferent nociceptors, would translate into improved efficacy at lower doses compared to a peripherally-restricted molecule (Minett et al., 2012; Dib-Hajj et al., 2013; Alexandrou et al., 2016). Our findings support the view that pharmacologic inhibition of peripheral $Na_V1.7$ channels will translate into pain mitigation in humans. $Na_V1.7$ antagonists currently undergoing clinical trials or in development may ultimately enable vigorous testing of this hypothesis (Emery et al., 2016).

Acknowledgements

The authors thank their colleagues Raymond Hurst for assistance in designing initial skin-nerve prep studies, Dr. Cheryl Stucky for guidance in implementing the skin-nerve prep technique, Chris Biorn and Jessica Able for surgical assistance with the skin-nerve prep, Cheng Su for statistical recommendations, Min-Hwa Jasmine Lin for pharmacokinetic guidance, Melanie Cooke and Roman Shimanovich for formulation support, Paul Rose for assistance with mouse and rat Na$_V$1.7 cell line generation, and Zaven Kaprielian for critical review of the manuscript.

Author contribution

Participated in research design: Fremeau, Ilch, Kornecook, Lehto, Matson, Moyer, Taborn, Weiss, Yin, Yu

Conducted experiments: Altmann, Be, Berry, Ilch, Jarosh, Johnson, Lee, Lehto, Ligutti, Luther, Liu, Matson, Ortuno, Roberts, Taborn, Wang, Yin, Zhu

Contributed new reagents: Weiss

Performed data analysis: Altmann, Be, Berry, Ilch, Jarosh, Johnson, Kornecook, Lee, Lehto, Ligutti, Lin, Luther, Liu, Matson, Moyer, Ortuno, Roberts, Taborn, Wang, Yin, Yu, Zhu

Wrote or contributed to manuscript writing: Kornecook, Ligutti, Liu, Luther, Moyer, Yin, Yu

References

Ahuja S, Mukund S, Deng L, Khakh K, Chang E, Ho H, Shriver S, Young C, Lin S, Johnson JP, Jr., Wu P, Li J, Coons M, Tam C, Brillantes B, Sampang H, Mortara K, Bowman KK, Clark KR, Estevez A, Xie Z, Verschoof H, Grimwood M, Dehnhardt C, Andrez JC, Focken T, Sutherlin DP, Safina BS, Starovasnik MA, Ortwine DF, Franke Y, Cohen CJ, Hackos DH, Koth CM and Payandeh J (2015) Structural basis of Nav1.7 inhibition by an isoform-selective small-molecule antagonist. *Science* **350**:aac5464.

Alexandrou AJ, Brown AR, Chapman ML, Estacion M, Turner J, Mis MA, Wilbrey A, Payne EC, Gutteridge A, Cox PJ, Doyle R, Printzenhoff D, Lin Z, Marron BE, West C, Swain NA, Storer RI, Stupple PA, Castle NA, Hounshell JA, Rivara M, Randall A, Dib-Hajj SD, Krafte D, Waxman SG, Patel MK, Butt RP and Stevens EB (2016) Subtype-Selective Small Molecule Inhibitors Reveal a Fundamental Role for Nav1.7 in Nociceptor Electrogenesis, Axonal Conduction and Presynaptic Release. *PloS one* **11**:e0152405.

Arendt-Nielsen L, Harris S, Whiteside GT, Hummel M, Knappenberger T, O'Keefe S, Kapil R and Kyle D (2016) A randomized, double-blind, positive-controlled, 3-way cross-over human experimental pain study of a TRPV1 antagonist (V116517) in healthy volunteers and comparison with preclinical profile. *Pain* **157**:2057-2067.

Bagal SK, Chapman ML, Marron BE, Prime R, Storer RI and Swain NA (2014) Recent progress in sodium channel modulators for pain. *Bioorganic & medicinal chemistry letters* **24**:3690-3699.

Basbaum AI, Bautista DM, Scherrer G and Julius D (2009) Cellular and molecular mechanisms of pain. *Cell* **139**:267-284.

Bautista DM, Wilson SR and Hoon MA (2014) Why we scratch an itch: the molecules, cells and circuits of itch. *Nature neuroscience* **17**:175-182.

Black JA, Frezel N, Dib-Hajj SD and Waxman SG (2012) Expression of Nav1.7 in DRG neurons extends from peripheral terminals in the skin to central preterminal branches and terminals in the dorsal horn. *Molecular pain* **8**:82.

Blair NT and Bean BP (2002) Roles of tetrodotoxin (TTX)-sensitive Na+ current, TTX-resistant Na+ current, and Ca2+ current in the action potentials of nociceptive sensory neurons. *The Journal of neuroscience : the official journal of the Society for Neuroscience* **22**:10277-10290.

Brochu RM, Dick IE, Tarpley JW, McGowan E, Gunner D, Herrington J, Shao PP, Ok D, Li C, Parsons WH, Stump GL, Regan CP, Lynch JJ, Jr., Lyons KA, McManus OB, Clark S, Ali Z, Kaczorowski GJ, Martin WJ and Priest BT (2006) Block of peripheral nerve sodium channels selectively inhibits features of neuropathic pain in rats. *Molecular pharmacology* **69**:823-832.

Cao L, McDonnell A, Nitzsche A, Alexandrou A, Saintot PP, Loucif AJ, Brown AR, Young G, Mis M, Randall A, Waxman SG, Stanley P, Kirby S, Tarabar S, Gutteridge A, Butt R, McKernan RM, Whiting P, Ali Z, Bilsland J and Stevens EB (2016) Pharmacological reversal of a pain phenotype in iPSC-derived sensory neurons and patients with inherited erythromelalgia. *Science translational medicine* **8**:335ra356.

Chiu IM, Barrett LB, Williams EK, Strochlic DE, Lee S, Weyer AD, Lou S, Bryman GS, Roberson DP, Ghasemlou N, Piccoli C, Ahat E, Wang V, Cobos EJ, Stucky CL, Ma Q, Liberles SD and Woolf CJ (2014) Transcriptional profiling at whole population and single cell levels reveals somatosensory neuron molecular diversity. *eLife* **3**.

Cox JJ, Reimann F, Nicholas AK, Thornton G, Roberts E, Springell K, Karbani G, Jafri H, Mannan J, Raashid Y, Al-Gazali L, Hamamy H, Valente EM, Gorman S, Williams R, McHale DP, Wood JN, Gribble FM and Woods CG (2006) An SCN9A channelopathy causes congenital inability to experience pain. *Nature* **444**:894-898.

Cummins TR, Howe JR and Waxman SG (1998) Slow closed-state inactivation: a novel mechanism underlying ramp currents in cells expressing the hNE/PN1 sodium channel. *The Journal of neuroscience : the official journal of the Society for Neuroscience* **18**:9607-9619.

Davidson S and Giesler GJ (2010) The multiple pathways for itch and their interactions with pain. *Trends in neurosciences* **33**:550-558.

de Lera Ruiz M and Kraus RL (2015) Voltage-Gated Sodium Channels: Structure, Function, Pharmacology, and Clinical Indications. *Journal of medicinal chemistry* **58**:7093-7118.

Deuis JR, Wingerd JS, Winter Z, Durek T, Dekan Z, Sousa SR, Zimmermann K, Hoffmann T, Weidner C, Nassar MA, Alewood PF, Lewis RJ and Vetter I (2016) Analgesic Effects of GpTx-1, PF-04856264 and CNV1014802 in a Mouse Model of NaV1.7-Mediated Pain. *Toxins* **8**.

Devigili G, Eleopra R, Pierro T, Lombardi R, Rinaldo S, Lettieri C, Faber CG, Merkies IS, Waxman SG and Lauria G (2014) Paroxysmal itch caused by gain-of-function Nav1.7 mutation. *Pain* **155**:1702-1707.

Dib-Hajj SD, Yang Y, Black JA and Waxman SG (2013) The Na(V)1.7 sodium channel: from molecule to man. *Nature reviews Neuroscience* **14**:49-62.

DiMauro EF, Altmann S, Berry LM, Bregman H, Chakka N, Chu-Moyer M, Bojic EF, Foti RS, Fremeau R, Gao H, Gunaydin H, Guzman-Perez A, Hall BE, Huang H, Jarosh M, Kornecook T, Lee J, Ligutti J, Liu D, Moyer BD, Ortuno D, Rose PE, Schenkel LB, Taborn K, Wang J, Wang Y, Yu V and Weiss MM (2016) Application of a Parallel Synthetic Strategy in the Discovery of Biaryl Acyl Sulfonamides as Efficient and Selective NaV1.7 Inhibitors. *Journal of medicinal chemistry* **59**:7818-7839.

Doherty EM, Fotsch C, Bannon AW, Bo Y, Chen N, Dominguez C, Falsey J, Gavva NR, Katon J, Nixey T, Ognyanov VI, Pettus L, Rzasa RM, Stec M, Surapaneni S, Tamir R, Zhu J, Treanor JJ and Norman MH (2007) Novel vanilloid receptor-1 antagonists: 2. Structure-activity relationships of 4-oxopyrimidines leading to the selection of a clinical candidate. *Journal of medicinal chemistry* **50**:3515-3527.

Emery EC, Luiz AP and Wood JN (2016) Nav1.7 and other voltage-gated sodium channels as drug targets for pain relief. *Expert opinion on therapeutic targets* **20**:975-983.

Faber CG, Hoeijmakers JG, Ahn HS, Cheng X, Han C, Choi JS, Estacion M, Lauria G, Vanhoutte EK, Gerrits MM, Dib-Hajj S, Drenth JP, Waxman SG and Merkies IS (2012) Gain of function Nanu1.7 mutations in idiopathic small fiber neuropathy. *Annals of neurology* **71**:26-39.

Fertleman CR, Baker MD, Parker KA, Moffatt S, Elmslie FV, Abrahamsen B, Ostman J, Klugbauer N, Wood JN, Gardiner RM and Rees M (2006) SCN9A mutations in paroxysmal extreme pain disorder: allelic variants underlie distinct channel defects and phenotypes. *Neuron* **52**:767-774.

Finnerup NB, Attal N, Haroutounian S, McNicol E, Baron R, Dworkin RH, Gilron I, Haanpaa M, Hansson P, Jensen TS, Kamerman PR, Lund K, Moore A, Raja SN, Rice AS, Rowbotham M, Sena E, Siddall P, Smith BH and Wallace M (2015) Pharmacotherapy for neuropathic pain in adults: a systematic review and meta-analysis. *The Lancet Neurology* **14**:162-173.

Focken T, Liu S, Chahal N, Dauphinais M, Grimwood ME, Chowdhury S, Hemeon I, Bichler P, Bogucki D, Waldbrook M, Bankar G, Sojo LE, Young C, Lin S, Shuart N, Kwan R, Pang J, Chang JH, Safina BS, Sutherlin DP, Johnson JP, Jr., Dehnhardt CM, Mansour TS, Oballa RM, Cohen CJ and Robinette CL (2016) Discovery of Aryl Sulfonamides as Isoform-Selective Inhibitors of NaV1.7 with Efficacy in Rodent Pain Models. *ACS medicinal chemistry letters* **7**:277-282.

Frost JM, DeGoey DA, Shi L, Gum RJ, Fricano MM, Lundgaard GL, El-Kouhen OF, Hsieh GC, Neelands T, Matulenko MA, Daanen JF, Pai M, Ghoreishi-Haack N, Zhan C, Zhang XF and Kort ME (2016) Substituted Indazoles as Nav1.7 Blockers for the Treatment of Pain. *Journal of medicinal chemistry* **59**:3373-3391.

Fukuoka T, Kobayashi K, Yamanaka H, Obata K, Dai Y and Noguchi K (2008) Comparative study of the distribution of the alpha-subunits of voltage-gated sodium channels in normal and axotomized rat dorsal root ganglion neurons. *The Journal of comparative neurology* **510**:188-206.

Fukuoka T and Noguchi K (2011) Comparative study of voltage-gated sodium channel alpha-subunits in non-overlapping four neuronal populations in the rat dorsal root ganglion. *Neuroscience research* **70**:164-171.

Gingras J, Smith S, Matson DJ, Johnson D, Nye K, Couture L, Feric E, Yin R, Moyer BD, Peterson ML, Rottman JB, Beiler RJ, Malmberg AB and McDonough SI (2014) Global Nav1.7 knockout mice recapitulate the phenotype of human congenital indifference to pain. *PloS one* **9**:e105895.

Goldberg YP, MacFarlane J, MacDonald ML, Thompson J, Dube MP, Mattice M, Fraser R, Young C, Hossain S, Pape T, Payne B, Radomski C, Donaldson G, Ives E, Cox J, Younghusband HB, Green R, Duff A, Boltshauser E, Grinspan GA, Dimon JH, Sibley BG, Andria G, Toscano E, Kerdraon J, Bowsher D, Pimstone SN, Samuels ME, Sherrington R and Hayden MR (2007) Loss-of-function mutations in the Nav1.7 gene underlie congenital indifference to pain in multiple human populations. *Clinical genetics* **71**:311-319.

Graceffa RF, Boezio AA, Able J, Altmann S, Berry LM, Boezio CM, Butler JR, Chu-Moyer MY, Cooke M, DiMauro EF, Dineen TA, Feric Bojic E, Foti RS, Fremeau RT, Jr., Guzman-Perez A, Gao H, Gunaydin H, Huang H, Huang L, Ilch C, Jarosh M, Kornecook T, Kreiman CR, La DS, Ligutti J, Milgram BC, Lin MJ, Marx IE, Nguyen HN, Peterson EA, Rescourio G, Roberts J, Schenkel LB, Shimanovich R, Sparling BA, Stellwagen J, Taborn K, Vaida KR, Wang J, Yeoman JT, Yu VL, Zhu D, Moyer BD and Weiss MM (2017) Sulfonamides as Selective NaV1.7 Inhibitors: Optimizing Potency, Pharmacokinetics, and Metabolic Properties to Obtain Atropisomeric Quinolinone (AM-0466) that Affords Robust In Vivo Activity. *Journal of medicinal chemistry*.

Hargreaves K, Dubner R, Brown F, Flores C and Joris J (1988) A new and sensitive method for measuring thermal nociception in cutaneous hyperalgesia. *Pain* **32**:77-88.

Haroutounian S, Nikolajsen L, Bendtsen TF, Finnerup NB, Kristensen AD, Hasselstrom JB and Jensen TS (2014) Primary afferent input critical for maintaining spontaneous pain in peripheral neuropathy. *Pain* **155**:1272-1279.

Ho C and O'Leary ME (2011) Single-cell analysis of sodium channel expression in dorsal root ganglion neurons. *Molecular and cellular neurosciences* **46**:159-166.

Hockley JR, Gonzalez-Cano R, McMurray S, Tejada-Giraldez MA, McGuire C, Torres A, Wilbrey AL, Cibert-Goton V, Nieto FR, Pitcher T, Knowles CH, Baeyens JM, Wood JN, Winchester WJ, Bulmer DC, Cendan CM and McMurray G (2017) Visceral and somatic pain modalities reveal NaV 1.7-independent visceral nociceptive pathways. *The Journal of physiology*.

Hoffmann T, Sauer SK, Horch RE and Reeh PW (2008) Sensory transduction in peripheral nerve axons elicits ectopic action potentials. *The Journal of neuroscience : the official journal of the Society for Neuroscience* **28**:6281-6284.

Holmes D (2016) The pain drain. *Nature* **535**:S2-3.

Klugbauer N, Lacinova L, Flockerzi V and Hofmann F (1995) Structure and functional expression of a new member of the tetrodotoxin-sensitive voltage-activated sodium channel family from human neuroendocrine cells. *The EMBO journal* **14**:1084-1090.

Knezevic NN, Cicmil N, Knezevic I and Candido KD (2015) Discontinued neuropathic pain therapy between 2009-2015. *Expert opinion on investigational drugs* **24**:1631-1646.

Koltzenburg M, Stucky CL and Lewin GR (1997) Receptive properties of mouse sensory neurons innervating hairy skin. *Journal of neurophysiology* **78**:1841-1850.

Kort ME, Atkinson RN, Thomas JB, Drizin I, Johnson MS, Secrest MA, Gregg RJ, Scanio MJ, Shi L, Hakeem AH, Matulenko MA, Chapman ML, Krambis MJ, Liu D, Shieh CC, Zhang X, Simler G, Mikusa JP, Zhong C, Joshi S, Honore P, Roeloffs R, Werness S, Antonio B, Marsh KC, Faltynek CR, Krafte DS,

Jarvis MF and Marron BE (2010) Subtype-selective Na(v)1.8 sodium channel blockers: identification of potent, orally active nicotinamide derivatives. *Bioorganic & medicinal chemistry letters* **20**:6812-6815.

Kwan KY, Glazer JM, Corey DP, Rice FL and Stucky CL (2009) TRPA1 modulates mechanotransduction in cutaneous sensory neurons. *The Journal of neuroscience : the official journal of the Society for Neuroscience* **29**:4808-4819.

Lennertz RC, Kossyreva EA, Smith AK and Stucky CL (2012) TRPA1 mediates mechanical sensitization in nociceptors during inflammation. *PloS one* **7**:e43597.

Liu D, Tseng M, Epstein LF, Green L, Chan B, Soriano B, Lim D, Pan O, Murawsky CM, King CT and Moyer BD (2016) Evaluation of recombinant monoclonal antibody SVmab1 binding to Na V1.7 target sequences and block of human Na V1.7 currents. *F1000Research* **5**:2764.

Liu Y and Ma Q (2011) Generation of somatic sensory neuron diversity and implications on sensory coding. *Current opinion in neurobiology* **21**:52-60.

Lotsch J, Oertel BG and Ultsch A (2014) Human models of pain for the prediction of clinical analgesia. *Pain* **155**:2014-2021.

Madeja M (2000) Do neurons have a reserve of sodium channels for the generation of action potentials? A study on acutely isolated CA1 neurons from the guinea-pig hippocampus. *The European journal of neuroscience* **12**:1-7.

Matson DJ, Hamamoto DT, Bregman H, Cooke M, DiMauro EF, Huang L, Johnson D, Li X, McDermott J, Morgan C, Wilenkin B, Malmberg AB, McDonough SI and Simone DA (2015) Inhibition of Inactive States of Tetrodotoxin-Sensitive Sodium Channels Reduces Spontaneous Firing of C-Fiber Nociceptors and Produces Analgesia in Formalin and Complete Freund's Adjuvant Models of Pain. *PloS one* **10**:e0138140.

McCormack K, Santos S, Chapman ML, Krafte DS, Marron BE, West CW, Krambis MJ, Antonio BM, Zellmer SG, Printzenhoff D, Padilla KM, Lin Z, Wagoner PK, Swain NA, Stupple PA, de Groot M, Butt RP and Castle NA (2013) Voltage sensor interaction site for selective small molecule inhibitors of voltage-gated sodium channels. *Proceedings of the National Academy of Sciences of the United States of America* **110**:E2724-2732.

Minett MS, Nassar MA, Clark AK, Passmore G, Dickenson AH, Wang F, Malcangio M and Wood JN (2012) Distinct Nav1.7-dependent pain sensations require different sets of sensory and sympathetic neurons. *Nature communications* **3**:791.

Nassar MA, Stirling LC, Forlani G, Baker MD, Matthews EA, Dickenson AH and Wood JN (2004) Nociceptor-specific gene deletion reveals a major role for Nav1.7 (PN1) in acute and inflammatory pain. *Proceedings of the National Academy of Sciences of the United States of America* **101**:12706-12711.

Oertel BG and Lotsch J (2013) Clinical pharmacology of analgesics assessed with human experimental pain models: bridging basic and clinical research. *British journal of pharmacology* **168**:534-553.

Pinto V, Derkach VA and Safronov BV (2008) Role of TTX-sensitive and TTX-resistant sodium channels in Adelta- and C-fiber conduction and synaptic transmission. *Journal of neurophysiology* **99**:617-628.

Pizzo PAC, N. M.; Carter-Pokras, O.; Christopher, M.; Farrar, J. T.; Follett, K. A.; Heitkemper, M. M.; Inturrisi, C.; Keefe, F.; Kerns, R. D.; Lee, J. S.; Loder, E.; Mackey, S.; Marinelli, R.; Payne, R.; Thernstrom, M.; Turk, D. C.; Wesselmann, U.; Zeltzer, L. (2011) Relieving Pain in America, A Blueprint for Transforming Prevention, Care, Education and Research. , in, Institute of Medicine Report from the Committee on Advancing Pain Research, Care, and Education, Washington, DC.

Renganathan M, Cummins TR and Waxman SG (2001) Contribution of Na(v)1.8 sodium channels to action potential electrogenesis in DRG neurons. *Journal of neurophysiology* **86**:629-640.

Rice FL, Albrecht PJ, Wymer JP, Black JA, Merkies IS, Faber CG and Waxman SG (2015) Sodium channel Nav1.7 in vascular myocytes, endothelium, and innervating axons in human skin. *Molecular pain* **11**:26.

Rush AM, Cummins TR and Waxman SG (2007) Multiple sodium channels and their roles in electrogenesis within dorsal root ganglion neurons. *The Journal of physiology* **579**:1-14.

Sun S, Cohen CJ and Dehnhardt CM (2014a) Inhibitors of voltage-gated sodium channel Nav1.7: patent applications since 2010. *Pharmaceutical patent analyst* **3**:509-521.

Sun S, Jia Q, Zenova AY, Chafeev M, Zhang Z, Lin S, Kwan R, Grimwood ME, Chowdhury S, Young C, Cohen CJ and Oballa RM (2014b) The discovery of benzenesulfonamide-based potent and selective inhibitors of voltage-gated sodium channel Na(v)1.7. *Bioorganic & medicinal chemistry letters* **24**:4397-4401.

Taylor NC, Sosa, M. P. (2013) Chronic pain, in *Pain Management Study*, Decision Resources.

Theile JW, Fuller MD and Chapman ML (2016) The selective Nav1.7 inhibitor, PF-05089771, interacts equivalently with fast and slow inactivated Nav1.7 channels. *Molecular pharmacology*.

Theriault O and Chahine M (2014) Correlation of the electrophysiological profiles and sodium channel transcripts of individual rat dorsal root ganglia neurons. *Frontiers in cellular neuroscience* **8**:285.

Usoskin D, Furlan A, Islam S, Abdo H, Lonnerberg P, Lou D, Hjerling-Leffler J, Haeggstrom J, Kharchenko O, Kharchenko PV, Linnarsson S and Ernfors P (2015) Unbiased classification of sensory neuron types by large-scale single-cell RNA sequencing. *Nature neuroscience* **18**:145-153.

Vetter I, Deuis JR, Mueller A, Israel MR, Starobova H, Zhang A, Rash LD and Mobli M (2016) NaV1.7 as a pain target - From gene to pharmacology. *Pharmacology & therapeutics*.

Weiss M, Boezio A, Boezio C, Butler JR, Chu-Moyer MY, DiMauro EF, Dineen T, Graceffa R, Guzman-Perez A, Huang H, Kreiman C, La D, Marx IE, Milgram BC, Nguyen HN, Peterson E, Romero K and Sparling B (2014) Bicyclic Sulfonamide Compounds as Sodium Channel Inhibitors. *PCT Int Appl* **WO2014201206**.

Yang Y, Wang Y, Li S, Xu Z, Li H, Ma L, Fan J, Bu D, Liu B, Fan Z, Wu G, Jin J, Ding B, Zhu X and Shen Y (2004) Mutations in SCN9A, encoding a sodium channel alpha subunit, in patients with primary erythermalgia. *Journal of medical genetics* **41**:171-174.

Zhang MM, Wilson MJ, Gajewiak J, Rivier JE, Bulaj G, Olivera BM and Yoshikami D (2013) Pharmacological fractionation of tetrodotoxin-sensitive sodium currents in rat dorsal root ganglion neurons by mu-conotoxins. *British journal of pharmacology* **169**:102-114.

Footnotes

This work was funded by Amgen, Inc.

[1] Stephen Altmann current address: Sanofi-Genzyme, 500 Kendall Square, Cambridge, MA 02142, United States

[2] Danny Ortuno current address: Novartis Institutes for BioMedical Research Inc., 250 Massachusetts Ave, Cambridge, MA 02139, United States

[3] Robert T. Fremeau Jr. current address: NeuroRx Consulting, 854 Massachusetts Avenue, Unit 3, MA 02139, United States

Figure Legends

Figure 1. Potent inhibition of TTX-S Na_V channel currents by AMG8379 but not AMG8380 in mouse DRG neurons. A. Structures of AMG8379 and AMG8380. B. Representative whole cell patch clamp recordings for active enantiomer AMG8379 (left) and less active enantiomer AMG8380 (right) showing reversible block of TTX-S Na_V channels. TTX was used as a positive control. C. Dose-response curves for AMG8379 and AMG8380 on TTX-S currents. AMG8379 IC_{50} was 3.1 ± 0.7 nM and AMG8380 was nearly one thousand-fold less potent with an IC_{50} of 2,560 ± 743 nM (n=4-6 neurons per compound). D. Representative whole cell patch clamp recordings for active enantiomer AMG8379 (left) and less active enantiomer AMG8380 (right) showing nominal block of TTX-R currents up to 5 uM. Recordings were performed in the presence of 500 nM TTX to block endogenous TTX-S currents. The positive control $Na_V1.8$ blocker (compound 31 from (Kort et al., 2010)) fully blocked TTX-R currents.

Figure 2. Mechanically-evoked action potential firing in C-fibers is blocked by TTX. A. Representative traces for fibers treated with control (0.1% DMSO) or TTX with the indicated force stimuli. B. Force-response curve. Mechanically-induced action potential firing was blocked by 1 uM TTX. **** $P < 0.0001$ by repeated measure two-way ANOVA compared to control. Mean ± SEM; n=25 fibers per group. C. TTX dose-dependent inhibition of mechanically-evoked action potential firing in C-fibers. Mechanical stimuli were 150 mN for 10 sec. Representative traces for control (0.1% DMSO; left) and TTX (right). D. Dose response curve with TTX.

JPET Fast Forward. Published on May 4, 2017 as DOI: 10.1124/jpet.116.239590
This article has not been copyedited and formatted. The final version may differ from this version.

Figure 3. Inhibition of mechanically-evoked action potential firing in TTX-sensitive C-fibers by AMG8379. A. Representative traces at 0 and 25 min for 0.1% DMSO control and increasing concentrations of AMG8379. Mechanical stimuli were 150 mN for 10 sec every 5 min. B. AMG8379 inhibition of action potential firing over time. ** $P < 0.01$, *** $P < 0.001$ by repeated measure two-way ANOVA with Dunnett's multiple comparison test compared to DMSO. Mean ± SEM; n=20-23 fibers per group. C. Dose-response curve with AMG8379 at the 25 minute time point. A baseline firing frequency of 0% was set to the level of mechanically-evoked action potential firing of C-fibers reported in the $Na_V1.7$ knockout mouse (Gingras et al., 2014).

Figure 4. Less active enantiomer AMG8380 does not block mechanically-evoked action potential firing in C-fibers. A. Representative traces for 470 nM AMG8379 and AMG8380 at 0 and 25 min post-compound addition. Mechanical stimuli were 150 mN for 10 sec every 5 min. B. Inhibition of action potential firing over time by AMG8379 but not AMG8380. *** $P < 0.001$ by repeated measure two-way ANOVA. Mean ± SEM; n=22-24 fibers per group.

Figure 5. Thermal-evoked action potential firing in C-fibers. A. Representative traces for fibers incubated with solutions at the indicated temperatures. B. Temperature-response curve. * $P < 0.05$, ** $P < 0.01$ and *** $P < 0.001$ by one-way ANOVA with

Dunnett's multiple comparison test compared to 30 ºC. Mean ± SEM; n=8 fibers per group.

Figure 6. Inhibition of thermal-evoked action potential firing of TTX-sensitive C-fibers by AMG8379. A. Representative traces for 470 nM AMG8379 and AMG8380 over time. Thermal stimuli were 48ºC for 10 sec every 5 min. TTX completely blocked action potential firing in response to thermal stimuli. B. Inhibition of action potential firing over time for fibers with a baseline (time zero) firing frequency >1 Hz at 48ºC. * $P < 0.05$ by repeated measure two-way ANOVA compared to AMG8380. Mean ± SEM; n=16 fibers per group.

Figure 7. Lack of inhibition of thermal-evoked action potential firing of TTX-resistant C-fibers by AMG8379 and AMG8380. A. Representative traces for 470 nM AMG8379 and AMG8380 over time. Thermal stimuli were 48ºC for 10 sec every 5 min. A $Na_V1.8$ blocker (1 μM) completely blocked action potential firing in response to thermal stimuli. B. No differential inhibition of action potential firing by AMG8379 or AMG8380 over time for fibers with a baseline (time zero) firing frequency >1 Hz at 48ºC. $P > 0.05$ by repeated measures two-way ANOVA. Mean ± SEM; n=12-15 fibers per group.

Figure 8. AMG8379 does not affect locomotor activity in mice at doses up to 100 mg/kg. Basic (horizontal) movement was quantified via automated beam break analysis

over a 30 min period 4 hours after oral compound administration. P > 0.05 by one-way ANOVA. Mean ± SEM; n= 10 per group.

Figure 9. Inhibition of histamine-induced scratching in mice by AMG8379 but not AMG8380. A. Total number of scratch bouts elicited over a 15 min test period following intradermal histamine injection. AMG8379 dose-dependently decreased scratch bouts. DPH = diphenhydramine (30 mg/kg); *** P < 0.001, **** P < 0.0001 compared to vehicle-treated group; one-way ANOVA followed by Dunnett's post hoc tests; Mean ± SEM; n = 10 for vehicle as well as AMG8379 groups and n = 8 for DPH group. B. Total number of scratch bouts elicited over a 15 min test period following intradermal histamine injection. AMG8380 did not decrease scratch bouts; one-way ANOVA, p > 0.05 compared to vehicle. AMG8379 dose = 100 mg/kg; *** P < 0.001 compared to vehicle-treated group; one-way ANOVA followed by Dunnett's post hoc tests; Mean ± SEM; n = 9-10 for vehicle and AMG8380 groups and n = 8 for AMG8379 group.

Figure 10. AMG8379 reduced UVB-induced thermal hyperalgesia and acute capsaicin-induced nociception in mice. A. Prior to compound treatment, paw withdrawal latency was measured for both the contralateral (contra) and ipsilateral (ipsi) hind paw in response to a thermal stimulus applied 48 hours following induction of a localized UVB burn injury. Following oral administration of AMG8379, AMG8380, naproxen (30 mg/kg), or vehicle, withdrawal latency was measured again for the ipsilateral paw. ** P < 0.01 and *** P < 0.001 compared to the post-drug ipsilateral vehicle-treated group;

one-way ANOVA followed by Dunnett's post hoc tests; Mean ± SEM; n = 10-12 per group. B. Total time spent engaged in paw licking behavior over a 5 min test session in response to an intradermal injection of capsaicin. Prior to capsaicin injection, mice were orally administered AMG8379, the selective TRPV1 antagonist AMG517, or a vehicle control. *** $P < 0.001$ compared to vehicle-treated group; one-way ANOVA followed by Dunnett's post hoc tests; Mean ± SEM; n = 9-10 per group.

JPET Fast Forward. Published on May 4, 2017 as DOI: 10.1124/jpet.116.239590
This article has not been copyedited and formatted. The final version may differ from this version.

Table 1

Antagonist activity of AMG8379 and AMG8380 at human, mouse, and rat $Na_V1.7$ channels. IC_{50} values are expressed as mean ± SEM. n= number of replicate experiments performed.

Channel	3078379 PX IC_{50} (μM)	3078380 PX IC_{50} (μM)
h$Na_V1.7$	0.0085 ± 0.025 (n=9)	0.907 ± 0.372 (n=8)
h$Na_V1.7$	0.5216 ± 0.075* (n=3)	12.92 ± 1.36* (n=3)
m$Na_V1.7$	0.0186 ± 0.0052 (n=3)	0.387 ± 0.049 (n=3)
r$Na_V1.7$	8.61 ± 0.242 (n=3)	>42 (n=3)
mDRG TTX-S	0.0031 ± 0.0007 (n=6)	2.56 ± 0.743 (n=4)
mDRG TTX-R	>5 (n=2)	>5 (n=2)
h$Na_V1.5$	>30 (n=2)	>30 (n=2)

PX, PatchXpress; h$Na_V1.7$, human $Na_V1.7$; m$Na_V1.7$, mouse $Na_V1.7$; r$Na_V1.7$, rat $Na_V1.7$; mDRG, mouse dorsal root ganglia; TTX-S, tetrodotoxin-sensitive; TTX-R, tetrodotoxin-resistant; h$Na_V1.5$, human $Na_V1.5$. * Compound potency determined on the resting/closed state.

JPET Fast Forward. Published on May 4, 2017 as DOI: 10.1124/jpet.116.239590
This article has not been copyedited and formatted. The final version may differ from this version.

Table 2

Antagonist activity of AMG8379 and AMG8380 at human and mouse Na_V channels. IC_{50} values are expressed as mean ± SEM. n= number of replicate experiments performed.

Channel	3078379 IWQ IC_{50} (μM)	3078380 IWQ IC_{50} (μM)
hNa_V1.1	>14 (n=3)	>14 (n=3)
hNa_V1.2	2.17 ± 0.07* (n=3)	> 30* (n=3)
hNa_V1.3	>14 (n=3)	>14 (n=3)
hNa_V1.4	>14 (n=3)	>14 (n=3)
hNa_V1.5	>14 (n=3)	>14 (n=3)
hNa_V1.6	1.31 ± 0.17 (n=4)	>10 (n=6)
hNa_V1.7	0.0032 ± 0.001 (n=5)	0.391 ± 0.160 (n=6)
mNa_V1.1	> 30* (n=3)	> 30* (n=3)
mNa_V1.6	2.74 ± 0.49* (n=3)	> 30* (n=3)
mNa_V1.7	0.0168 ± 0.005 (n=4)	0.681 ± 0.258 (n=7)

IWQ, IonWorks Quattro; hNa_V1.1, human Na_V1.1; hNa_V1.2, human Na_V1.2; hNa_V1.3, human Na_V1.3; hNa_V1.4, human Na_V1.4; hNa_V1.5, human Na_V1.5; hNa_V1.6, human Na_V1.6; hNa_V1.7, human Na_V1.7; mNa_V1.1, mouse Na_V1.1; mNa_V1.6, mouse Na_V1.6; mNa_V1.7, mouse Na_V1.7. *Compound potency determined by manual patch clamp electrophysiology using the IWQ voltage protocol.

JPET Fast Forward. Published on May 4, 2017 as DOI: 10.1124/jpet.116.239590
This article has not been copyedited and formatted. The final version may differ from this version.

Table 3.

Terminal plasma concentrations and target coverage multiples over the mNa$_V$1.7 IC_{50} (C_u/mPX IC_{50}) for AMG8379 and AMG8380 from behavioral experiments. Values in bold indicate target coverage multiples that significantly affected behavioral endpoints. Values are expressed as mean ± SEM.

Experiment	Compound	Dose (mg/kg)	[Plasma] (μM)	[Plasma] C_u (μM)	C_u/mPX IC_{50}
Open-field activity (Fig. 8)	AMG8379	10	13.7 ± 0.766	0.024 ± 0.001	1.7 ± 0.09
	AMG8379	30	47.1 ± 2.45	0.081 ± 0.004	5.84 ± 0.305
	AMG8379	100	189.4 ± 13.3	0.326 ± 0.023	23.5 ± 1.65
Histamine (Fig. 9A)	AMG8379	10	10.6 ± 1.14	0.018 ± 0.002	1.32 ± 0.141
	AMG8379	30	42.7 ± 8.26	0.073 ± 0.014	**5.3 ± 1.03**
	AMG8379	100	174.1 ± 7.98	0.3 ± 0.014	**21.6 ± 0.99**
Histamine (Fig. 9B)	AMG8380	10	5.31 ± 0.848	0.073 ± 0.012	0.18 ± 0.030
	AMG8380	30	33.8 ± 4.96	0.466 ± 0.068	1.20 ± 0.177
	AMG8380	100	123.2 ± 7.92	1.70 ± 0.109	4.39 ± 0.283
	AMG8379	100	120.7 ± 4.29	0.207 ± 0.007	14.9 ± 0.527
UVB (Fig. 10A)	AMG8379	10	25.1 ± 5.84	0.043 ± 0.010	3.11 ± 0.723
	AMG8379	30	88.6 ± 8.67	0.153 ± 0.015	10.9 ± 1.08
	AMG8379	100	186.0 ± 16.1	0.321 ± 0.028	**23.1 ± 1.98**
	AMG8380	100	190.8 ± 19.6	2.63 ± 0.271	6.80 ± 0.699
Capsaicin (Fig. 10B)	AMG8379	30	55.7 ± 2.73	0.096 ± 0.005	6.90 ± 0.339
	AMG8379	100	171.1 ± 16.2	0.295 ± 0.028	**21.2 ± 2.01**

JPET Fast Forward. Published on May 4, 2017 as DOI: 10.1124/jpet.116.239590
This article has not been copyedited and formatted. The final version may differ from this version.

C_u, free drug concentration; histamine, histamine-induced scratch; UVB, UVB-induced thermal hyperalgesia; capsaicin, capsaicin-induced licking. AMG8379: f_u = 0.245%; mNa_V1.7 IC_{50} (PatchXpress) = 0.0186 μM. AMG8380: f_u = 1.38%; mNa_V1.7 IC_{50} (PatchXpress) = 0.387μM.

JPET Fast Forward. Published on May 4, 2017 as DOI: 10.1124/jpet.116.239590
This article has not been copyedited and formatted. The final version may differ from this version.

Fig 1

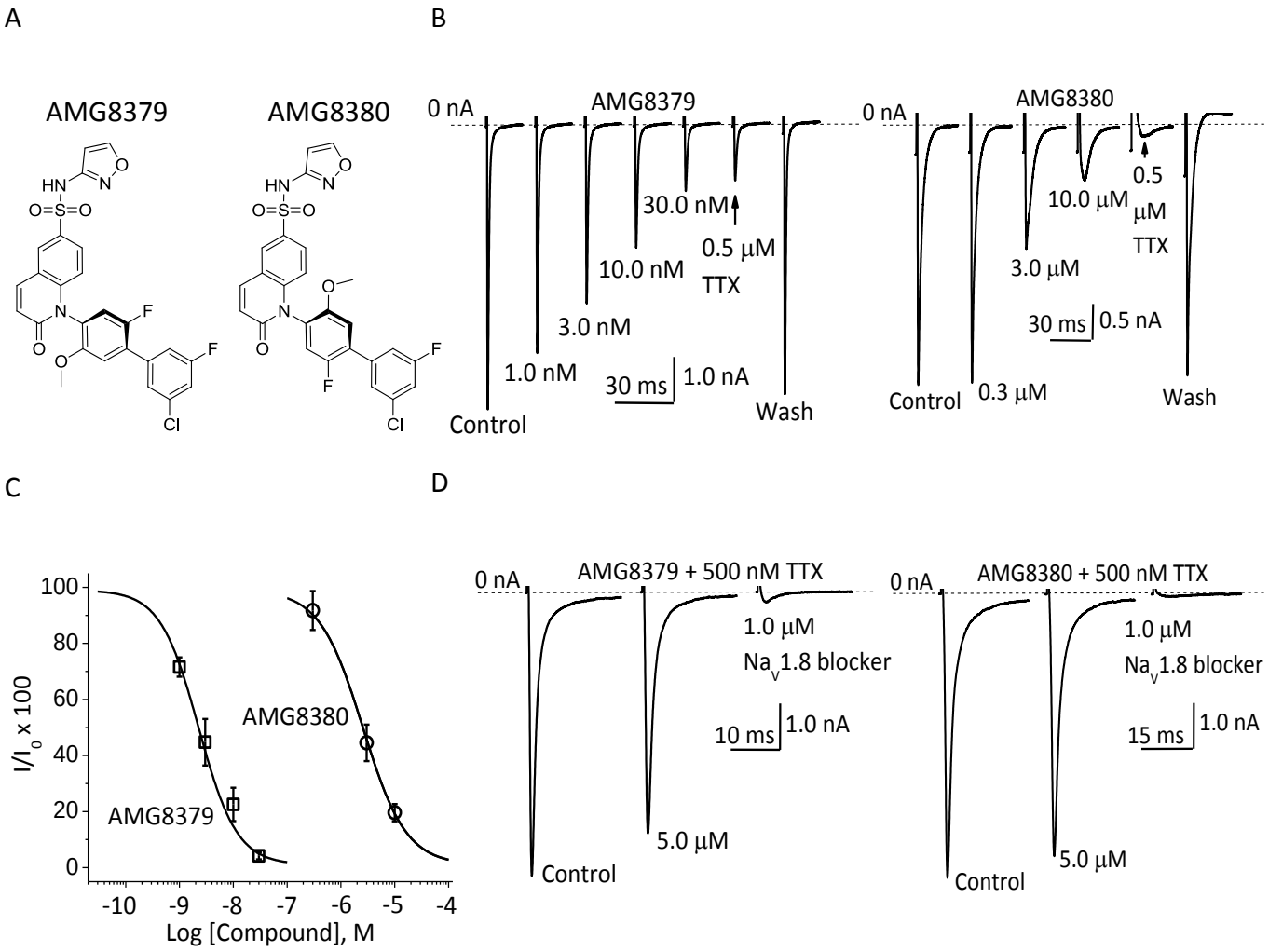

JPET Fast Forward. Published on May 4, 2017 as DOI: 10.1124/jpet.116.239590
This article has not been copyedited and formatted. The final version may differ from this version.

Fig 2

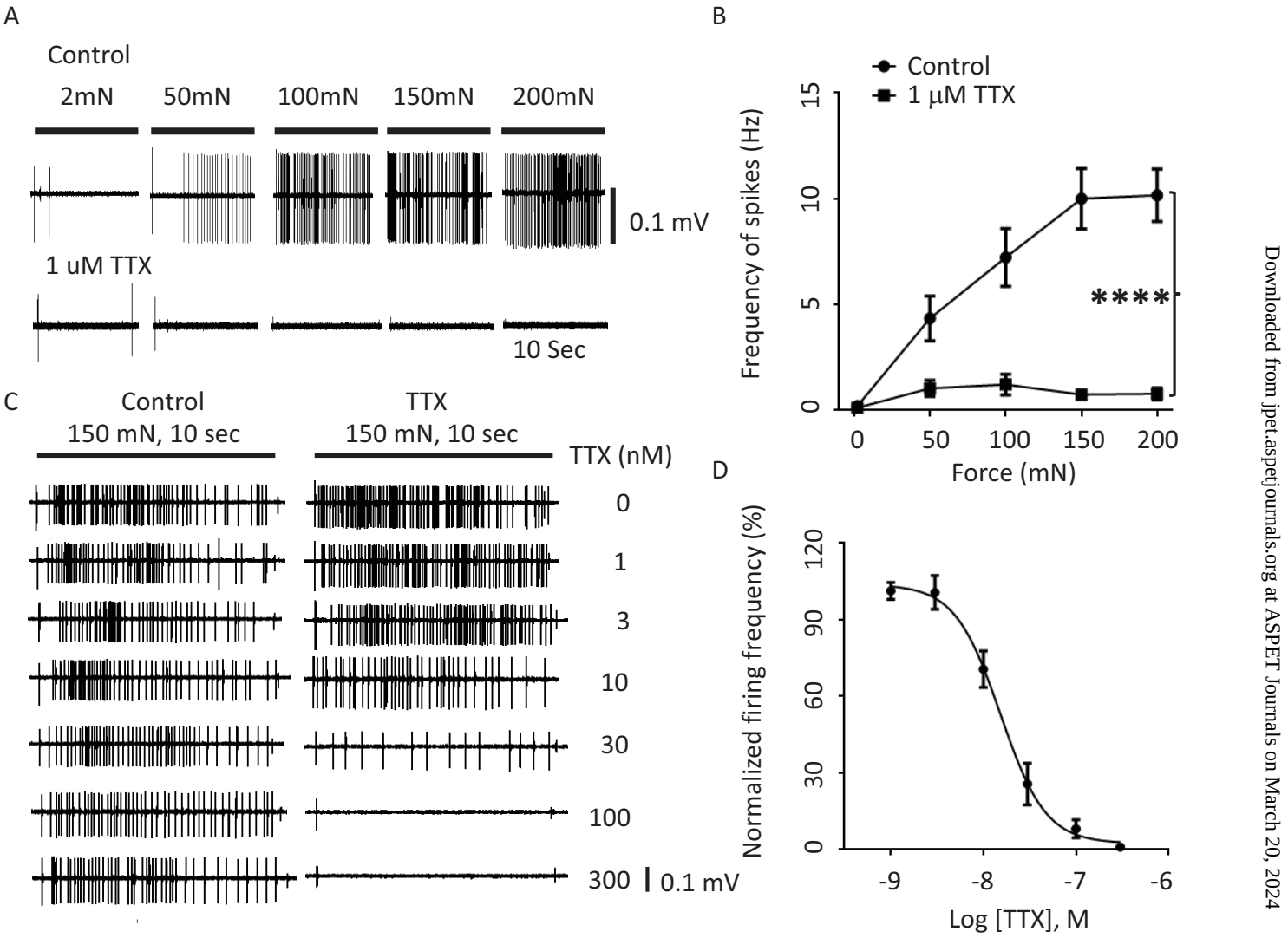

JPET Fast Forward. Published on May 4, 2017 as DOI: 10.1124/jpet.116.239590
This article has not been copyedited and formatted. The final version may differ from this version.

Fig 3

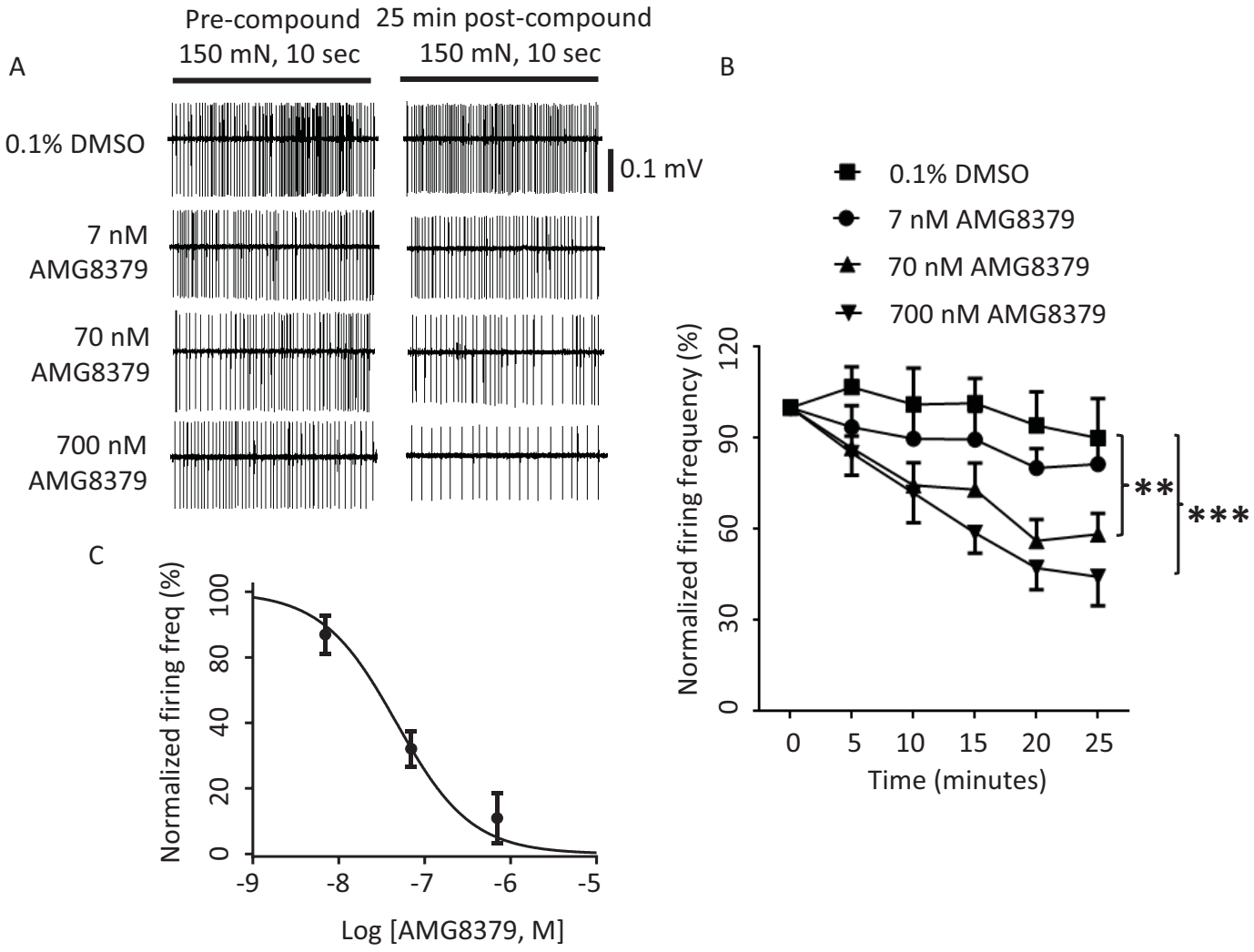

JPET Fast Forward. Published on May 4, 2017 as DOI: 10.1124/jpet.116.239590
This article has not been copyedited and formatted. The final version may differ from this version.

Fig 4

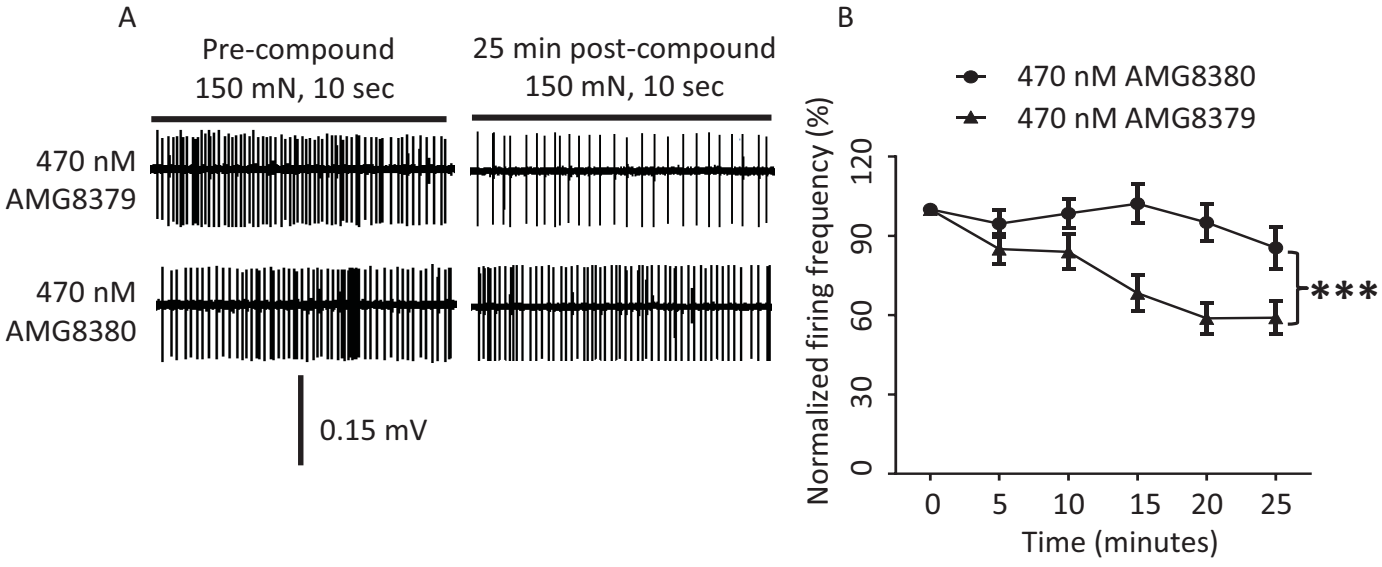

JPET Fast Forward. Published on May 4, 2017 as DOI: 10.1124/jpet.116.239590
This article has not been copyedited and formatted. The final version may differ from this version.

Fig 5

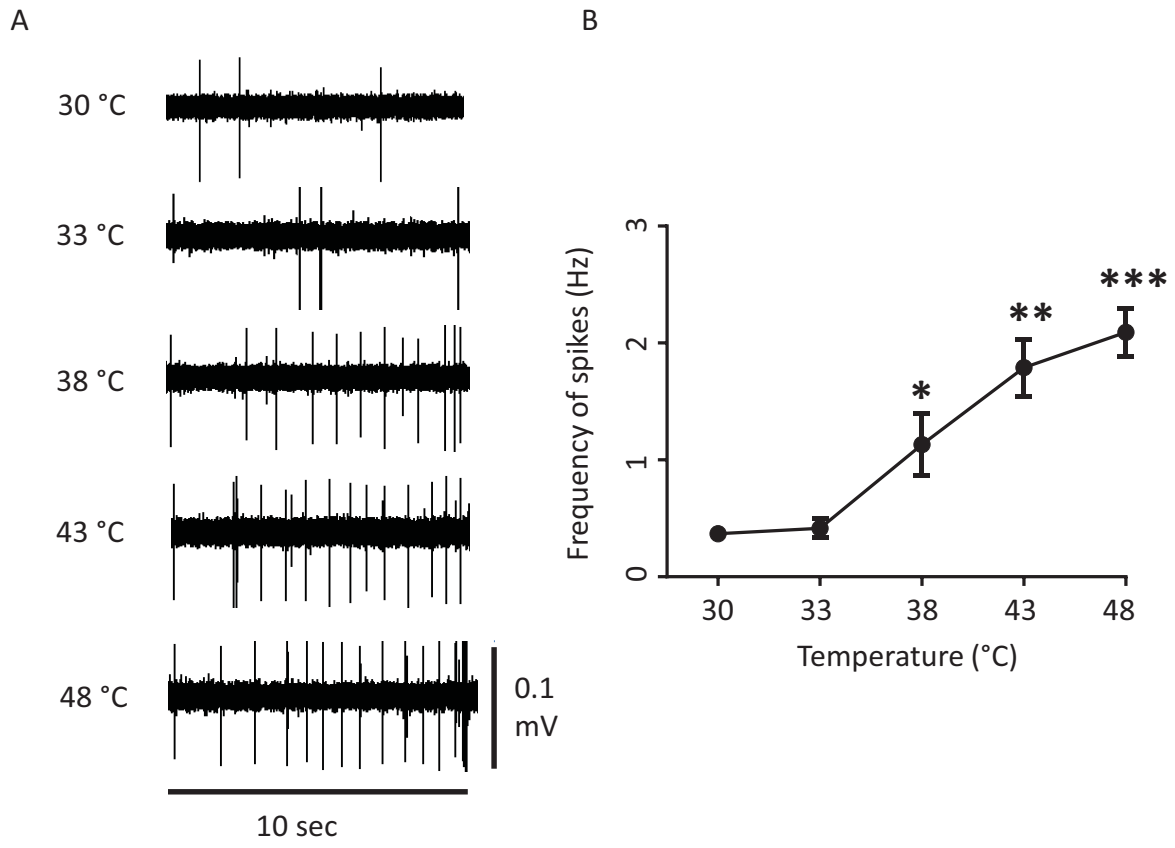

JPET Fast Forward. Published on May 4, 2017 as DOI: 10.1124/jpet.116.239590
This article has not been copyedited and formatted. The final version may differ from this version.

Fig 6

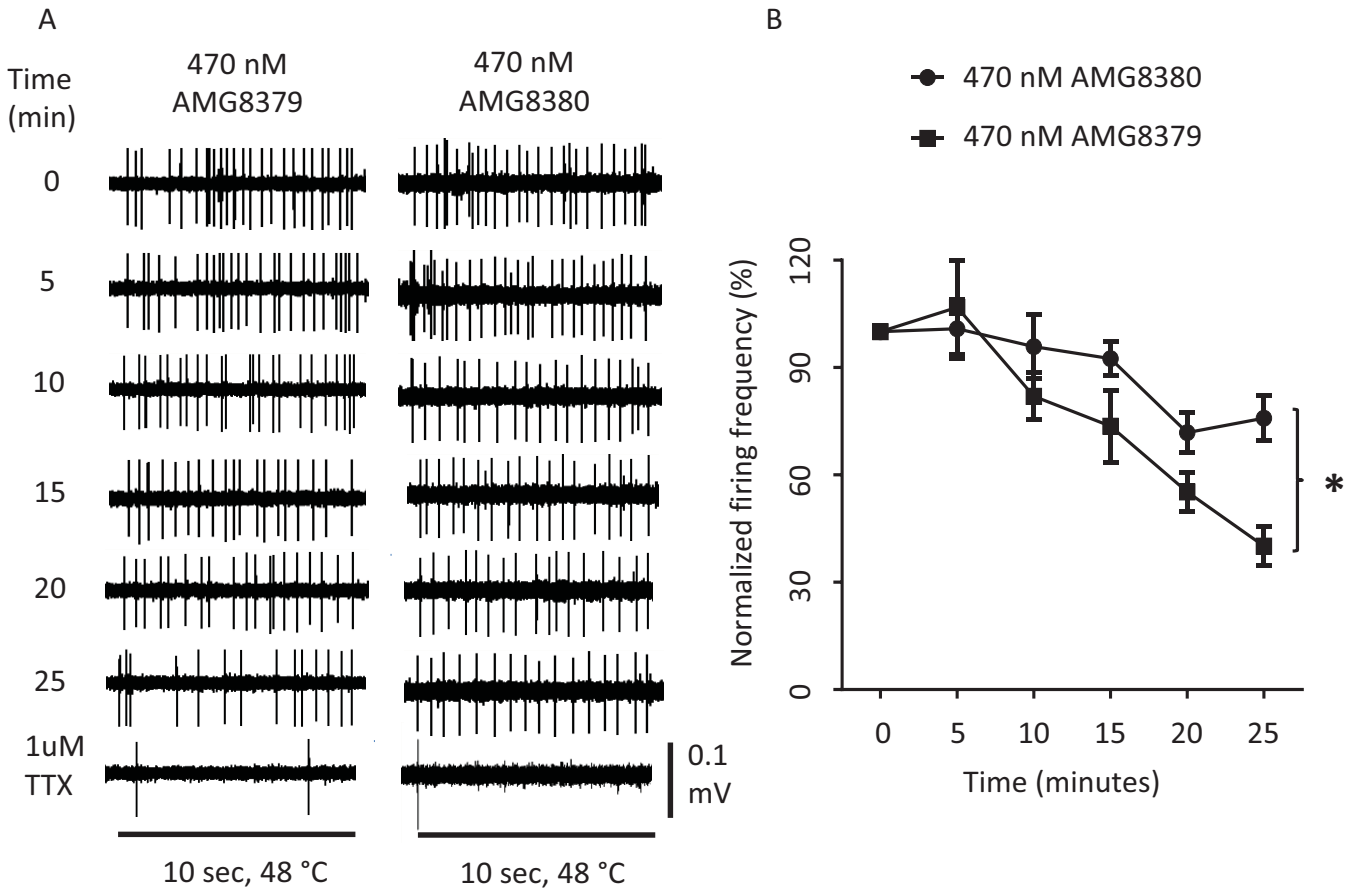

JPET Fast Forward. Published on May 4, 2017 as DOI: 10.1124/jpet.116.239590
This article has not been copyedited and formatted. The final version may differ from this version.

Fig 7

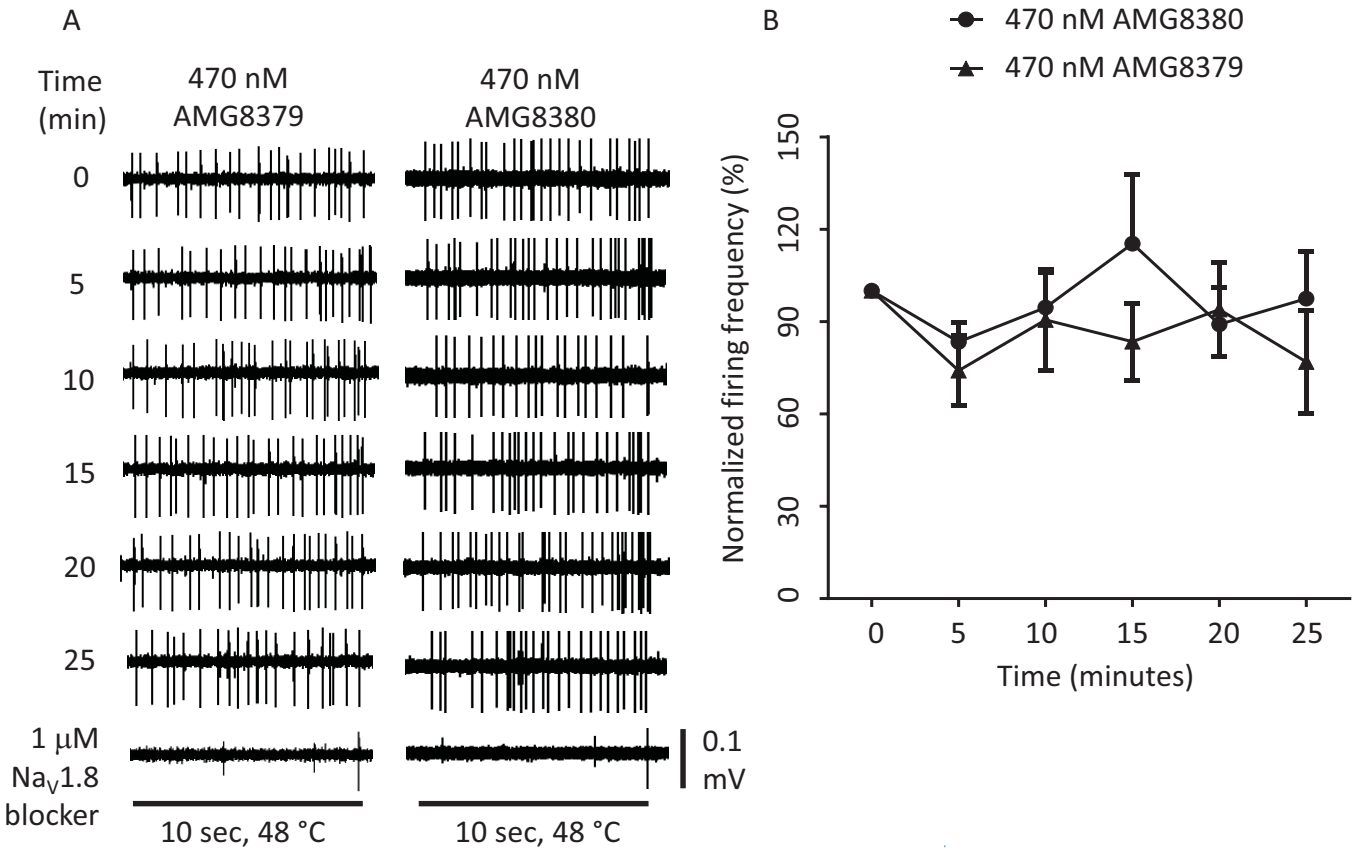

JPET Fast Forward. Published on May 4, 2017 as DOI: 10.1124/jpet.116.239590
This article has not been copyedited and formatted. The final version may differ from this version.

Fig 8

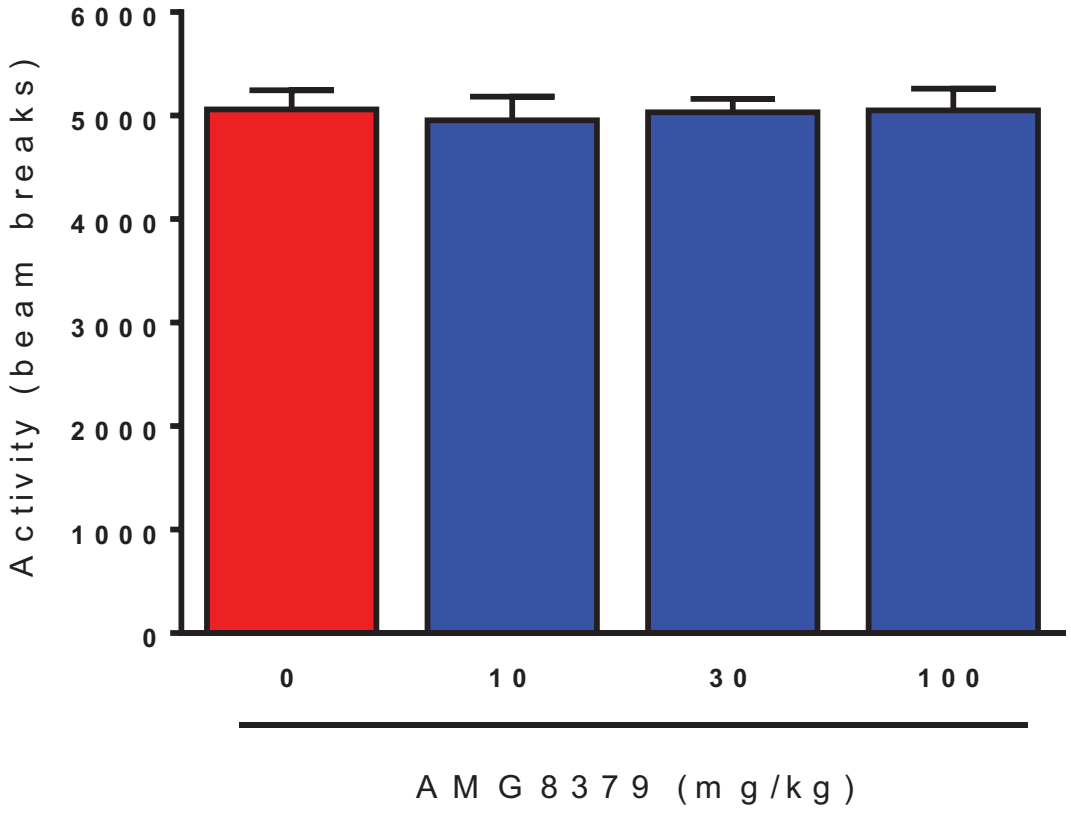

JPET Fast Forward. Published on May 4, 2017 as DOI: 10.1124/jpet.116.239590
This article has not been copyedited and formatted. The final version may differ from this version.

Fig 9

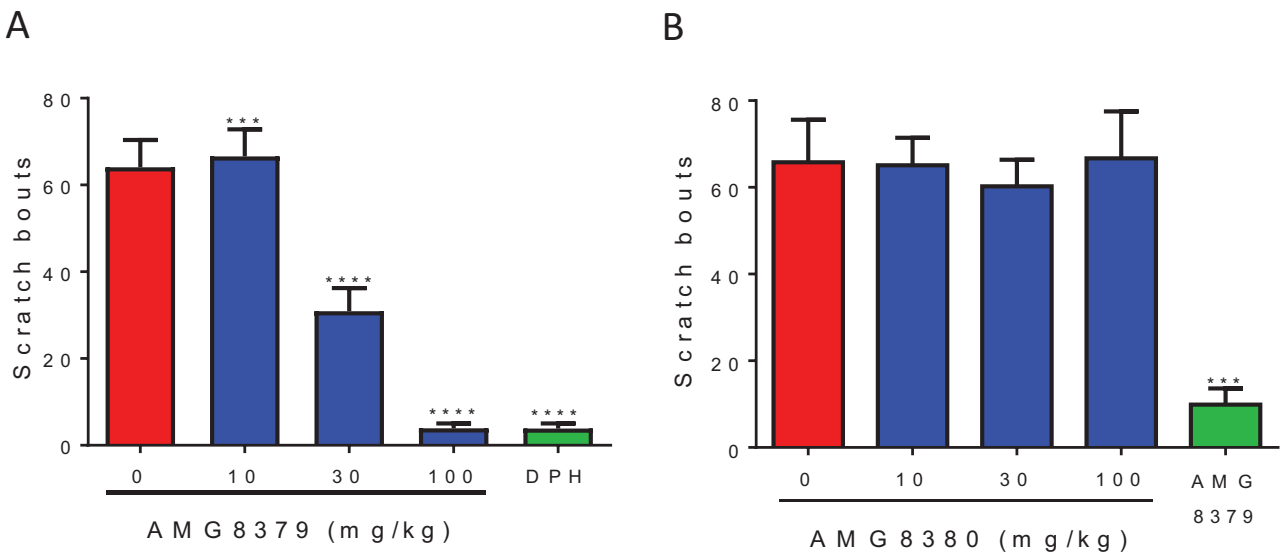

JPET Fast Forward. Published on May 4, 2017 as DOI: 10.1124/jpet.116.239590
This article has not been copyedited and formatted. The final version may differ from this version.

Fig 10

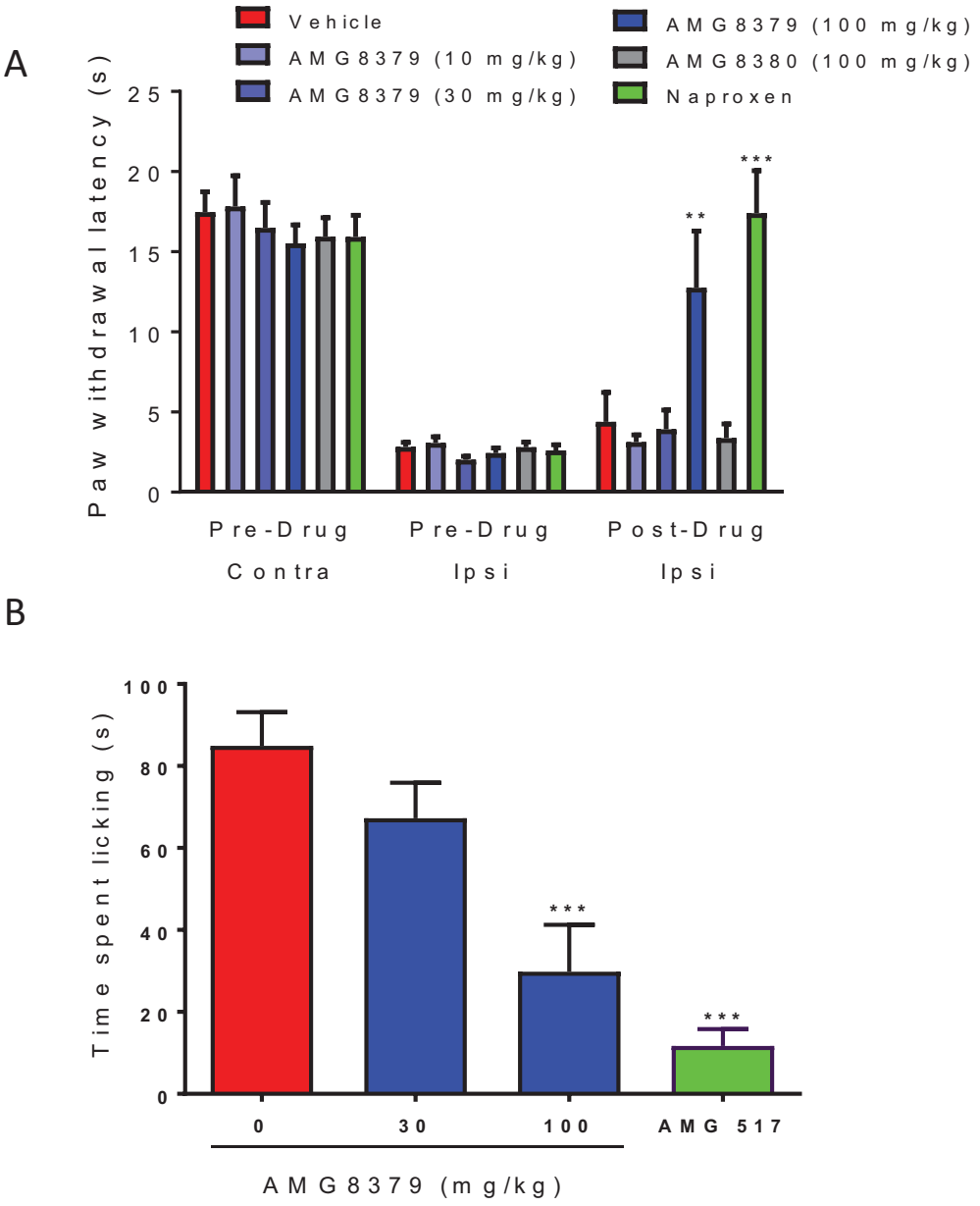

Supplementary Information

The Journal of Experimental Pharmacology and Experimental Therapeutics

Pharmacologic Characterization of AMG8379, a Potent and Selective Small Molecule Sulfonamide Antagonist of the Voltage-Gated Sodium Channel $Na_V1.7$

Thomas Kornecook, Ruoyuan Yin, Stephen Altmann, Xuhai Be, Virginia Berry, Christopher P. Ilch, Michael Jarosh, Danielle Johnson, Josie H. Lee, Sonya G. Lehto, Joseph Ligutti, Dong Liu, Jason Luther, David Matson, Danny Ortuno, John Roberts, Kristin Taborn, Jinti Wang, Matthew M. Weiss, Violeta Yu, Dawn X. D. Zhu, Robert T. Fremeau Jr., and Bryan D. Moyer

AMG8379

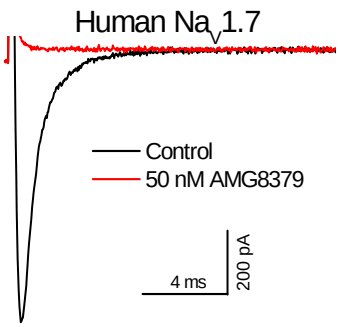

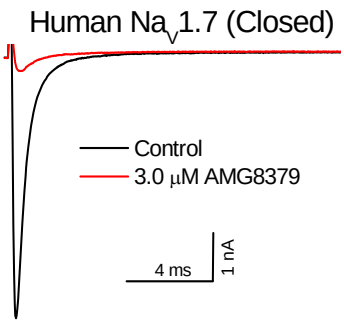

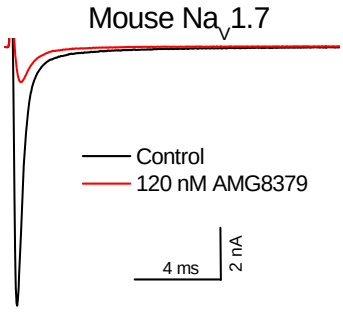

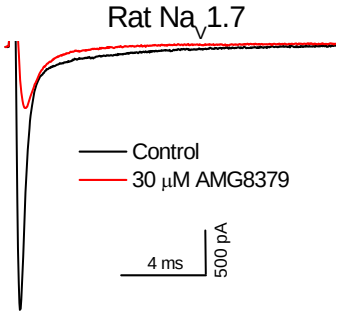

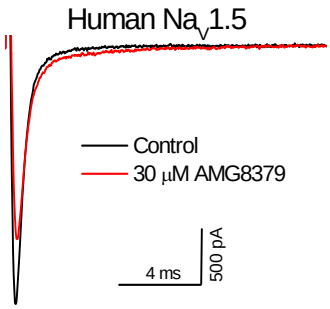

AMG8380

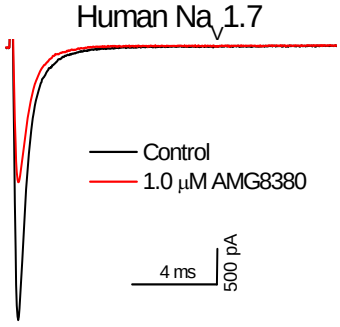

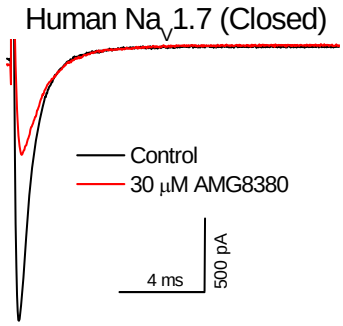

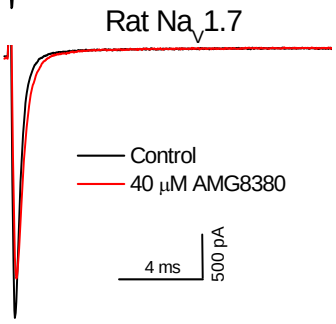

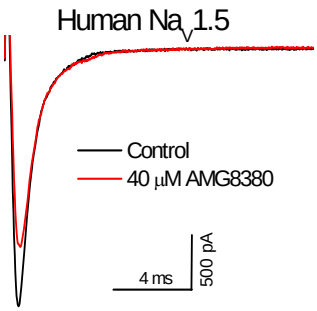

Supplementary Figure 1. Representative current traces illustrating potent and selective block of hNa_V1.7 and mNa_V1.7 but not rNa_V1.7 or hNa_V1.5 in a partially inactivated state or hNa_V1.7 channels in the resting/closed state by AMG8379 compared to AMG8380 in heterologous cells. Patch clamp recordings were from the PatchXpress platform. Traces show currents for the indicted channel before (black) and after (red) compound addition at the indicated concentrations.

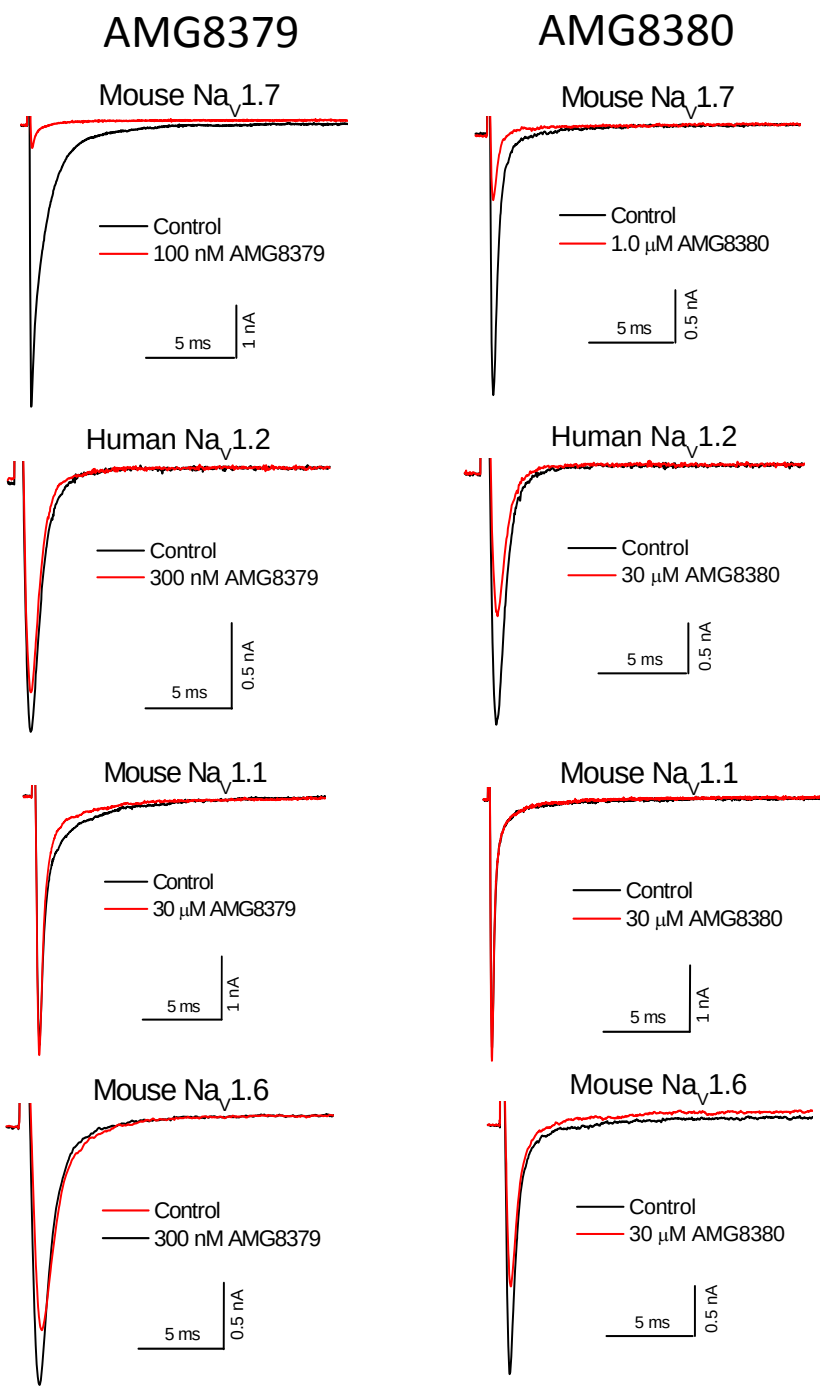

Supplementary Figure 2. Representative current traces illustrating potent and selective block of mNa$_V$1.7, but not hNa$_V$1.2, mNa$_V$1.1, and mNa$_V$1.6, channels by AMG8379 compared to AMG8380 in heterologous cells. Manual patch clamp electrophysiology recordings used the IonWorks Quattro voltage protocol. Traces show currents for the indicted channel before (black) and after (red) compound addition at the indicated concentrations.